symmetry

MDPI

Article

Parameter Identification in Nonlinear Vibrating Systems Using Runge–Kutta Integration and Levenberg–Marquardt Regression

Şefika İpek Lök [1], Ömer Ekim Genel [2], Rosario La Regina [3], Carmine Maria Pappalardo [4,*] and Domenico Guida [4]

[1] Defense Industries Research and Development Institute, Scientific and Technological Research Council of Türkiye (TÜBİTAK), Ankara 06105, Türkiye; sefika.lok@tubitak.gov.tr
[2] Altayçeşme mah. Sarıgül sk. 9B, Maltepe, İstanbul 34843, Türkiye; omerekim.genel@gmail.com
[3] MEID4, Research Center for AI-Based Innovation, 84091 Battipaglia, Salerno, Italy; rlaregina@unisa.it
[4] Department of Industrial Engineering, University of Salerno, Via Giovanni Paolo II 132, 84084 Fisciano, Salerno, Italy; guida@unisa.it
* Correspondence: cpappalardo@unisa.it

Abstract

Guided by principles of symmetry to achieve a proper balance among model consistency, accuracy, and complexity, this paper proposes a new approach for identifying the unknown parameters of nonlinear one-degree-of-freedom mechanical systems using nonlinear regression methods. To this end, the steps followed in this study can be summarized as follows. Firstly, given a proper set of input time histories and a virtual model with all parameters known, the dynamic response of the mechanical system of interest, used as output data, is evaluated using a numerical integration scheme, such as the classical explicit fixed-step fourth-order Runge–Kutta method. Secondly, the numerical values of the unknown parameters are estimated using the Levenberg–Marquardt nonlinear regression algorithm based on these inputs and outputs. To demonstrate the effectiveness of the proposed approach through numerical experiments, two benchmark problems are considered, namely a mass-spring-damper system and a simple pendulum-damper system. In both mechanical systems, viscous damping is included at the kinematic joints, whereas dry friction between the bodies and the ground is accounted for and modeled using the Coulomb friction force model. While the source of nonlinearity is the frictional interaction alone in the first benchmark problem, the finite rotation of the pendulum introduces geometric nonlinearity, in addition to the frictional interaction, in the second benchmark problem. To ensure symmetry in explaining model behavior and the interpretability of numerical results, the analysis presented in this paper utilizes five different input functions to validate the proposed method, representing the initial phase of ongoing research aimed at applying this identification procedure to more complex mechanical systems, such as multibody and robotic systems. The numerical results from this research demonstrate that the proposed approach effectively identifies the unknown parameters in both benchmark problems, even in the presence of nonlinear, time-varying external input actions.

Keywords: theoretical and applied mechanics; engineering mechanics; nonlinear dynamics; mechanical vibrations; numerical integration; nonlinear regression; system identification; viscous damping; dry friction

Check for updates

Academic Editor: George Karabatsos

Received: 11 October 2025
Revised: 14 December 2025
Accepted: 17 December 2025
Published: 21 December 2025

Copyright: © 2025 by the authors. Licensee MDPI, Basel, Switzerland. This article is an open access article distributed under the terms and conditions of the Creative Commons Attribution (CC BY) license.

1. Introduction

1.1. General Background

Dynamic modeling and structural identification are extensively used in civil, mechanical, and aerospace engineering to better understand and control structural systems [1–3]. These methods also play a prominent role in model updating, where finite element models are refined using measured vibration data to enhance accuracy [4,5]. For example, this combined approach is crucial in structural health monitoring, where it enables the detection, localization, and quantification of damage in bridges, buildings, and aircraft [6,7]. Additionally, dynamic modeling and structural identification support vibration control and mitigation by designing strategies such as tuned mass dampers, and they are essential in seismic and wind engineering for evaluating performance under extreme loads and predicting potential failure modes [8,9]. Beyond immediate performance assessment, finding a proper dynamical model of a structural system contributes to life-cycle evaluation by guiding maintenance planning, improving reliability, and ensuring overall safety and security [10]. Furthermore, another important aspect related to the engineering application of system identification methods in industry is predicting the remaining useful life of mechanical parts and structural elements, such as roller bearings or electromechanical components, by using variational mode decomposition techniques [11,12].

Accurate modeling and analysis of mechanical systems are essential steps for evaluating their responses under various realistic conditions [13–17]. In modeling of mechanical systems of engineering interest, quite often the numerical values of some parameters of the system model under consideration may not be known a priori [18–22]. In such cases, it is generally required to carry out experimental studies to estimate the numerical values of these unknown system parameters [23,24]. For instance, the inclusion of damping values of materials used in the system into the mathematical model is only possible by determining these numerical values obtained from dynamic tests in many cases. A similar approach is also required for the friction interaction that occurs between bodies moving relative to each other [25–27]. This is because it is very difficult, if not impossible, to devise a reliable method to make sensible predictions on the numerical values of the parameters describing the viscous damping and dry friction behavior.

1.2. Literature Review

The identification of joint damping and friction parameters plays a primary role in controlling robotic manipulators [28–30]. This task represents the first step of the friction compensation process, which improves transient performance and reduces steady-state error [31–33]. The use of identification techniques is also employed in the analysis of flexible structures, where one aims to accurately estimate the natural frequencies and damping ratios associated with the predominant normal modes. With the help of a modeling process that utilizes experimental data, mathematical models that are capable of representing the actual system behavior more accurately can be developed. For instance, to identify the equivalent stiffness coefficient of the system as a function of the mass and modal parameters, a numerical procedure is proposed and implemented in [34,35].

The extensive number of research papers in the literature on the various applications of dynamic modeling and structural identification methods highlights the significance of this topic in the broad field of mechanical and industrial engineering [36,37]. For example, the emerging areas where system identification methods appear to hold great promise are precision vehicle systems [38,39], trains [40], airplanes [41,42], agriculture machines [43,44], shear building systems [45–48], and robotic manipulators [49–52]. Essentially, dynamic modeling and system identification serve as the key connection between observed dy-

namic behavior and analytical models, allowing for effective diagnosis, prediction, and optimization of structural performance [53,54].

One of the methods that can be used to identify unknown system parameters, such as viscous damping and friction coefficient, is nonlinear regression. In this vein, this investigation explores the use of this approach in conjunction with the implementation of numerical methods for approximating solutions to nonlinear ordinary differential equations. Generally speaking, regression methods offer a robust framework for parameter estimation of mechanical systems by fitting a model to observed data. The various optimization techniques mainly used within this framework are the gradient descent method, the Gauss-Newton method, and the Levenberg–Marquardt method [55–58]. Each method has its strengths, but the Levenberg–Marquardt method is particularly noteworthy [59,60]. It is often favored in the literature due to its ability to strike a balance between the fast convergence of the Gauss-Newton method and the stability of the gradient descent method.

1.3. Scope and Contributions

This paper proposes a novel approach to establish a numerical framework that employs the Runge–Kutta numerical integration method [61,62] and the Levenberg–Marquardt iterative regression algorithm [63,64] to identify the viscous damping parameter and the dry friction coefficient in nonlinear vibrating system models. The new approach introduced in this investigation follows a general strategy inspired by the main idea behind adjoint analysis, which is used for control design in computational mechanics of rigid and deformable systems [65,66]. This approach was initially aimed at bypassing the use of model reduction methods and the necessity of solving the complete Riccati equation corresponding to the linear-quadratic regulator, which is numerically intractable for large systems [67,68]. More specifically, this paper utilizes the explicit fourth-order Runge–Kutta method and the Levenberg–Marquardt method for parameter estimation in single-degree-of-freedom nonlinear mechanical systems.

The paper first introduces the mathematical details of the new algorithm developed in this investigation. Subsequently, two numerical examples based on simple benchmark systems are analyzed to verify the performance of the proposed approach through numerical experiments. In the first benchmark problem, a mass-spring-damper system is considered, thereby accounting for the friction interaction between the cart and the prismatic joint connected to the ground. The second benchmark problem investigates a simple pendulum-damper system in the presence of friction interaction between the pendulum and the revolute joint attached to the ground. Thus, this study emphasizes the effectiveness and accuracy of the adopted approach in estimating unknown parameters such as viscous damping and friction coefficients. The authors aim to contribute to ongoing research in dynamic system modeling, offering insights that can be applied to more complex, multi-input, multi-output, and multibody mechanical systems in future work.

Driven by the principle of symmetry to maintain a balanced trade-off among model consistency, accuracy, and complexity, this paper presents a novel approach for identifying unknown parameters in nonlinear single-degree-of-freedom mechanical systems using nonlinear regression and time-marching numerical integration. In the context of the present work, the principle of symmetry means that two complementary demonstrative examples are analyzed under large displacements, namely a translational vibrating system and a rotational vibrating system, both described by nonlinear dynamical models. As discussed in detail below, the benchmark systems studied in this paper are a mass-spring-damper system and a simple pendulum-damper system, both subjected to dry friction. Furthermore, to preserve symmetry in interpreting model behavior and enhance the clarity of the numerical analysis of the benchmark system, five distinct input functions are used to

validate the proposed method, thereby effectively demonstrating its performance through numerical experiments.

In the paper, to demonstrate the effectiveness of the nonlinear identification procedure developed in this work for the two benchmark systems considered, dynamical simulations are performed from the beginning using two mechanical models: (a) a first model based on the actual numerical values of the parameter vector; (b) a second model based on an estimation of the numerical values of the parameter vector. In the second model, the numerical values employed to estimate the actual parameter vector are iteratively updated from an initial guess, gradually improving the current estimate. When the nonlinear regression method described in the paper is correctly implemented, the estimated parameter vector converges to the actual parameter vector. Thus, the performance of the methodology devised in this work is evaluated through extensive numerical experiments that compare, across different scenarios, the reference dynamic behaviors of the original benchmark systems with those obtained using the estimated set of system parameters.

In summary, this study presents a simulation-based framework for identifying unknown parameters in nonlinear mechanical systems. To evaluate the proposed method, numerical outputs are generated from a dynamical model with known parameters using explicit fourth-order Runge–Kutta integration, driven by prescribed input time histories. These outputs and inputs are then used to estimate the parameters through Levenberg–Marquardt nonlinear regression. The novelty of the present paper lies not in the Runge–Kutta numerical integration method or the Levenberg–Marquardt regression method by themselves, which are well-known numerical algorithms, but in their combined use to develop a simple yet effective parameter identification procedure that is suitable to estimate the numerical values of the physical parameters of mechanical systems described by nonlinear dynamical models.

To conclude, the new approach proposed here is validated across five typical time histories used as external excitations and applied to two benchmark systems, namely, a mass-spring-damper with Coulomb dry friction and a simple pendulum experiencing both frictional and geometric nonlinearities. The numerical results demonstrate reliable parameter identification even under nonlinear, time-varying external forces, emphasizing the robustness of the proposed method and supporting its application to more complex multibody or robotic mechanical systems.

1.4. Manuscript Organization

Apart from Section 1, the rest of the paper is organized according to the following structure. Section 2 introduces the fundamental steps of the Levenberg–Marquardt algorithm, which is the nonlinear regression method employed in this study. Section 3 explains the general workflow of the nonlinear parameter identification process devised in this paper, together with a short recall of the well-known fourth-order explicit Runge–Kutta scheme. Sections 4 and 5 respectively describe details of the first and second benchmark problems analyzed in this work. Section 6 presents the numerical results for both benchmark problems and discusses the effectiveness of the approach adopted in this investigation. Finally, Section 7 concludes the paper by summarizing the work done in this study, highlighting the main results obtained, and indicating future directions of research.

2. Nonlinear Regression Method

The Levenberg–Marquardt nonlinear regression algorithm is a useful optimization technique for solving nonlinear least-squares estimation problems. It combines the advantages of the Gauss-Newton method and the gradient descent technique, offering a more

robust solution approach that balances between speed and stability [69–72]. The key steps necessary for the computer implementation of this numerical method are summarized below.

A nonlinear model of a generic deterministic process can be written as follows:

$$\mathbf{Y}^i = f(\mathbf{X}^i, \mathbf{b}) + \boldsymbol{\varepsilon}^i, \quad i = 1, 2, \ldots, M \tag{1}$$

where M refers to the number of samples used for the discretization, $f(\mathbf{X}^i, \mathbf{b})$ designates the nonlinear function describing the system model of interest [55], $\mathbf{X}^i$ identifies the ith component of the input vector $\mathbf{X}$ of dimensions $M \times 1$, $\mathbf{Y}^i$ expresses ith component of the output vector $\mathbf{Y}$ of dimensions $M \times 1$, $\mathbf{b}$ stands for the vector of unknown parameters of the system model having dimensions $n_b \times 1$, and $\boldsymbol{\varepsilon}^i$ is the ith component of a stochastic error vector $\boldsymbol{\varepsilon}$ of dimensions $M \times 1$ that represents the model uncertainties with an expected value $E[\varepsilon^i] = 0$.

In the Levenberg–Marquardt algorithm, the nonlinear function $f(\mathbf{X}^i, \mathbf{b})$ acts as a parameterized mathematical model of the system of interest that must match its actual observations $\mathbf{Y}^i$ corresponding to a given input $\mathbf{X}^i$. The process gradually improves the parameter estimates $\mathbf{b}$ to reduce the sum of squared residuals, which are the differences between the measured data and the model predictions, as shown below. This iterative optimization is essential because, unlike linear models, the parameters of nonlinear models cannot be found through a direct analytical solution.

To implement a least-squares estimation, one can write the following equation:

$$S(\mathbf{b}) = \sum_{i=1}^{M} \left(\boldsymbol{e}^i(\mathbf{b}) \right)^2 \tag{2}$$

being:

$$\boldsymbol{e}^i(\mathbf{b}) = \mathbf{Y}^i - f(\mathbf{X}^i, \mathbf{b}) \tag{3}$$

where $S(\mathbf{b})$ refers to the sum of the squares of the ith deviations $\boldsymbol{e}^i(\mathbf{b})$ of the actual ith measurements $\mathbf{Y}^i$ from the ones predicted by the system model $f(\mathbf{X}^i, \mathbf{b})$ in correspondence of the ith input $\mathbf{X}^i$ using the set of system parameters $\mathbf{b}$. Clearly, the sum of squares $S(\mathbf{b})$ is the total obtained by squaring each number in a set and then adding all those squared values together. In general, this is a fundamental concept in statistics and algebra, used to measure the dispersion of data points or to illustrate relationships between numbers. In the current context, the sum of squares $S(\mathbf{b})$ denotes an overall metric of how well the system model function $f(\mathbf{X}^i, \mathbf{b})$ fits the input-output data $\mathbf{X}^i$ and $\mathbf{Y}^i$ based on a given parameter vector $\mathbf{b}$.

In practical applications, an iterative numerical method is often required to minimize the sum of the squares $S(\mathbf{b})$ by letting the argument of the parameter vector $\mathbf{b}$ vary in a given interval. Therefore, the unknown parameter vector $\mathbf{b}$ is replaced in each iteration step by a new estimation denoted with $\mathbf{b} + \Delta\mathbf{b}$. To mathematically obtain $\Delta\mathbf{b}$, the function $f(\mathbf{X}^i, \mathbf{b} + \Delta\mathbf{b})$ can be approximated with its first-order Taylor expansion as follows:

$$f(\mathbf{X}^i, \mathbf{b} + \Delta\mathbf{b}) \approx f(\mathbf{X}^i, \mathbf{b}) + \frac{\partial f}{\partial \mathbf{b}}(\mathbf{X}^i, \mathbf{b})\Delta\mathbf{b} = f(\mathbf{X}^i, \mathbf{b}) + \mathbf{J}_i \Delta\mathbf{b} \tag{4}$$

where $\mathbf{J}_i = \partial f(\mathbf{X}^i, \mathbf{b}) / \partial \mathbf{b}$ represents the Jacobian matrix of the system model function having dimensions $1 \times n_b$. Consequently, the sum of the squares of the deviations denoted with $S(\mathbf{b})$ can be written for the next iteration as follows:

$$S(\mathbf{b} + \Delta\mathbf{b}) = \sum_{i=1}^{M} \left(\mathbf{Y}^i - f(\mathbf{X}^i, \mathbf{b} + \Delta\mathbf{b}) \right)^2 \tag{5}$$

which leads to:

$$S(\mathbf{b}+\Delta\mathbf{b}) \approx \sum_{i=1}^{M}\left(\mathbf{Y}^i - f(\mathbf{X}^i,\mathbf{b}) - \mathbf{J}_i\Delta\mathbf{b}\right)^2 \tag{6}$$

Considering the Taylor expansion truncated at the first order provided in Equation (4), Equation (6) can be written in vector notation as given below:

$$S(\mathbf{b}+\Delta\mathbf{b}) = \|\mathbf{Y}-\mathbf{f}(\mathbf{X},\mathbf{b})-\mathbf{J}\Delta\mathbf{b}\|^2 = (\mathbf{Y}-\mathbf{f}(\mathbf{X},\mathbf{b})-\mathbf{J}\Delta\mathbf{b})^T(\mathbf{Y}-\mathbf{f}(\mathbf{X},\mathbf{b})-\mathbf{J}\Delta\mathbf{b}) \tag{7}$$

Taking the partial derivative of the approximation of $S(\mathbf{b}+\Delta\mathbf{b})$ with respect to $\Delta\mathbf{b}$ reported in matrix form in Equation (7), and setting it to zero, reduces to:

$$\frac{\partial S(\mathbf{b}+\Delta\mathbf{b})}{\partial\Delta\mathbf{b}} = -\mathbf{J}^T(\mathbf{Y}-\mathbf{f}(\mathbf{X},\mathbf{b})-\mathbf{J}\Delta\mathbf{b}) = \mathbf{0} \tag{8}$$

It follows that:

$$\mathbf{J}^T\mathbf{J}\Delta\mathbf{b} = \mathbf{J}^T(\mathbf{Y}-\mathbf{f}(\mathbf{X},\mathbf{b})) \tag{9}$$

In the Levenberg–Marquardt algorithm, a proper damping factor is added to the coefficient matrix of the linear system of algebraic equations given in Equation (9) as follows:

$$\left(\mathbf{J}^T\mathbf{J}+\lambda\mathbf{I}\right)\Delta\mathbf{b} = \mathbf{J}^T(\mathbf{Y}-\mathbf{f}(\mathbf{X},\mathbf{b})) \tag{10}$$

where λ denotes an artificial damping factor and $\mathbf{I}$ denotes the identity matrix of dimensions $n_b \times n_b$. Numerically solving in an iterative fashion the modified version of the linear system of algebraic equations provided in Equation (10) eventually leads to an approximated solution for the Newton difference vector $\Delta\mathbf{b}$ and, therefore, to the estimation of the vector of model parameters $\mathbf{b}$.

In engineering applications, the damping factor λ of the Levenberg–Marquardt algorithm is adjusted at each iteration in which Equation (10) is numerically solved. More specifically, when $S(\mathbf{b}+\Delta\mathbf{b})$ decreases rapidly, a smaller λ is used, giving a step closer to the Gauss-Newton method. Conversely, if an iteration results in an insufficient reduction in the residual, λ is increased, bringing the iterative step closer to the gradient descent method.

It is worth noting that, in Equation (1), $f(\mathbf{X}^i,\mathbf{b})$ represents a nonlinear function describing a deterministic process, while $\boldsymbol{\varepsilon}^i$ stands for the ith component of a stochastic error term with a zero expected value. Therefore, Equation (1) is conceived for reconstructing a desired output vector $\mathbf{Y}^i$ starting from a preassigned input vector $\mathbf{X}^i$ and a given vector of physical parameters $\mathbf{b}$ that one wants to estimate. By doing so, the error term $\boldsymbol{\varepsilon}^i$ serves as a random disturbance affecting the output measurements, thereby reproducing the realistic scenario of sensor-induced measurement noise, as mentioned before. On the other hand, as discussed in detail below in the paper, when Equation (1) is used in conjunction with a numerical integration scheme for performing dynamic simulations, such as the case of the numerical experiments considered in this study, there is no need to artificially account for the measurement noise error term $\boldsymbol{\varepsilon}^i$ since this is inherent to the numerical integration process, leading to a small but persistent accumulation of computational errors.

3. Nonlinear Parametric Identification

3.1. Nonlinear Systems Modeling

To implement the approach proposed in this investigation, one must first derive the configuration-space equations of motion for the mechanical system under study using the Lagrange equations of the second kind [73]. In Lagrangian mechanics, the set of Euler-Lagrange equations assumes the following matrix form:

$$\frac{d}{dt}\left(\frac{\partial T}{\partial \dot{\mathbf{q}}}\right)^T - \left(\frac{\partial T}{\partial \mathbf{q}}\right)^T + \left(\frac{\partial R}{\partial \dot{\mathbf{q}}}\right)^T + \left(\frac{\partial U}{\partial \mathbf{q}}\right)^T = \left(\frac{\delta W_{e,nc}^*}{\delta \mathbf{q}}\right)^T \tag{11}$$

where t is time, $\mathbf{q}$ denotes the system generalized coordinate vector of dimensions $n_q \times 1$, T is the system total kinetic energy, R identifies the system total Rayleigh dissipation function, U represents the system total potential energy, and $\delta W_{e,nc}^*$ is the system total virtual work associated with the external nonconservative mechanical actions that cannot be expressed as a function of a scalar quantity, such as the Rayleigh dissipation function [74,75]. By mathematically implementing Equation (11) and by respectively denoting the number of generalized coordinates with n_q, the number of state variables with $n_z = 2n_q$, and the number of inputs with n_u, one obtains:

$$\begin{cases} \mathbf{M}(\mathbf{q}, t)\ddot{\mathbf{q}} = \mathbf{Q}_b(\mathbf{q}, \dot{\mathbf{q}}, t) + \mathbf{B}_u(\mathbf{q}, t)\mathbf{u} \\ \mathbf{q}(0) = \mathbf{p}_0 \\ \dot{\mathbf{q}}(0) = \mathbf{v}_0 \end{cases} \tag{12}$$

where $\mathbf{p}_0$ and $\mathbf{v}_0$ respectively represent preassigned vectors of dimensions $n_q \times 1$ containing the system generalized positions and velocities that serve as initial conditions, whereas $\mathbf{M}(\mathbf{q}, t)$ represents the system mass matrix of dimensions $n_q \times n_q$, $\mathbf{Q}_b(\mathbf{q}, \dot{\mathbf{q}}, t)$ identifies the total system generalized force vector of dimensions $n_q \times 1$, $\mathbf{B}_u(\mathbf{q}, t)$ is the input influence matrix of dimensions $n_q \times n_u$, and $\mathbf{u}$ denotes the system input vector of dimensions $n_u \times 1$.

In the mathematical modeling of the nonlinear systems of interest in this investigation, it is fundamental to describe the dry friction phenomenon adequately. Adopting a Lagrangian approach based on multibody dynamics theory, the presence of dry friction is reflected in the total generalized force vector acting on the mechanical system under study [76,77]. More specifically, one can write $\mathbf{Q}_b(\mathbf{q}, \dot{\mathbf{q}}, t) = \mathbf{Q}_v(\mathbf{q}, \dot{\mathbf{q}}, t) + \mathbf{Q}_e(\mathbf{q}, \dot{\mathbf{q}}, t)$ and $\mathbf{Q}_e(\mathbf{q}, \dot{\mathbf{q}}, t) = \mathbf{Q}_{e,c}(\mathbf{q}, t) + \mathbf{Q}_{e,nc}(\mathbf{q}, \dot{\mathbf{q}}, t)$, where $\mathbf{Q}_v(\mathbf{q}, \dot{\mathbf{q}}, t)$ is the Coriolis and centrifugal generalized force vector of dimensions $n_q \times 1$, $\mathbf{Q}_e(\mathbf{q}, \dot{\mathbf{q}}, t)$ is the total external generalized force vector of dimensions $n_q \times 1$, $\mathbf{Q}_{e,c}(\mathbf{q}, t)$ is the conservative generalized force vector of dimensions $n_q \times 1$, and $\mathbf{Q}_{e,nc}(\mathbf{q}, \dot{\mathbf{q}}, t)$ is the nonconservative generalized force vector of dimensions $n_q \times 1$, where the latter accounts for friction forces. Therefore, the virtual work of the dry friction forces acting on the specific vibrating system analyzed is used to analytically determine the friction contribution to the total nonconservative generalized force vector.

As is well known, in Coulomb-based friction force models for dry friction, the term representing the Coulomb friction force is expressed as a sign function. However, this creates a discontinuity at zero relative velocity and, therefore, several regularization techniques that replace the sign function with a continuous function have been proposed in the literature to address this issue in computer implementation [78,79]. This is because the Coulomb term implemented via the sign function of velocity is nondifferentiable and may hinder a correct description of vibrational behavior near stick-slip. Thus, using a smooth surrogate or a light Stribeck regularization could aid convergence, thereby improving the expected behavior near zero velocity and any implications for convergence, as discussed in the literature [80].

On the other hand, when analyzing the key aspects of computer modeling in the SIMSCAPE MULTIBODY simulation environment available in MATLAB (https://mathworks.com), there are functional blocks with integrated static friction force models that allow for the simultaneous analysis of viscous friction, the smooth Coulomb friction model, and the Stribeck effect, resulting in realistic numerical outcomes in comparison with the MATLAB computations [81,82]. However, because the two benchmark problems examined in this study are simple nonlinear systems, numerical experiments show that the MATLAB

implementation of the sign function is sufficient to accurately capture the overall nonlinear vibrational behavior of the systems of interest, ignoring more complex behaviors such as the discontinuity near zero velocity and the Stribeck effect.

3.2. Nonlinear Integration Method

In this study, the key idea is to derive the input and output arrays to be used in the nonlinear regression method explained in Section 2 by performing time-domain numerical simulations of the dynamical model describing a nonlinear mechanical system of interest. In contrast to the conventional use of the regression approach, which employs experimentally obtained input and output arrays, the approach proposed and adopted in this paper requires the generation of input and output data through computer simulations, with the aim of performing parameter identification of nonlinear system models. In practical applications, computer-simulated data can be replaced with experimental measurements, thereby enabling the implementation of the proposed approach for nonlinear system identification.

In this approach, the continuous-time mathematical model is converted into its discrete-time dynamical counterpart by using a time discretization based on an even spacing of time intervals Δt. To this end, one can write:

$$t^i = (i-1)\Delta t, \quad i = 1, 2, \ldots, l \tag{13}$$

where N is the number of the discrete points forming the time grid excluding the zero, $l = N + 1$ is the actual dimensional length of the time grid, and $T_s = N\Delta t$ is the total time span of the dynamical simulation. By doing so, the simulation time span is first discretized into fixed interval time points. Thus, the input array can be constructed from the input force data, which accepts the time array as an argument, as given below:

$$\mathbf{U} = \begin{bmatrix} \mathbf{U}^1 \\ \mathbf{U}^2 \\ \vdots \\ \mathbf{U}^i \\ \vdots \\ \mathbf{U}^{l-1} \\ \mathbf{U}^l \end{bmatrix} \tag{14}$$

where $\mathbf{U}^i$ refers to the value of the input force vector of dimensions $n_u \times 1$ at the discrete time point t^i and $\mathbf{U}$ is a column vector of dimensions $ln_u \times 1$. The input array employed in the regression method is, therefore, the vector $\mathbf{X} = \mathbf{U}$ having dimensions $M \times 1$, where $M = ln_u$.

On the other hand, the output array is derived from the components of the state vector, which are obtained by solving the state equations. To perform numerical simulations, Equation (12), which is expressed in the configuration space, is transformed into the state space as follows:

$$\begin{cases} \dot{\mathbf{z}} = \mathbf{g}(\mathbf{z}, \mathbf{u}, t) \\ \mathbf{z}(0) = \mathbf{z}_0 \end{cases} \tag{15}$$

where $\mathbf{z}$ is the system state vector of dimensions $n_z \times 1$, $\mathbf{z}_0$ is a preassigned vector of dimensions $n_z \times 1$ defining the initial state, and $\mathbf{g}$ is the system state function of dimensions $n_z \times 1$, respectively defined as given below:

$$\mathbf{z} = \begin{bmatrix} \mathbf{q} \\ \dot{\mathbf{q}} \end{bmatrix}, \quad \mathbf{z}_0 = \begin{bmatrix} \mathbf{p}_0 \\ \mathbf{v}_0 \end{bmatrix} \tag{16}$$

and

$$\mathbf{g}(\mathbf{z},\mathbf{u},t)=\begin{bmatrix}\dot{\mathbf{q}}\\ \ddot{\mathbf{q}}\end{bmatrix}=\begin{bmatrix}\dot{\mathbf{q}}\\ \mathbf{M}^{-1}(\mathbf{q},t)(\mathbf{Q}_b(\mathbf{q},\dot{\mathbf{q}},t)+\mathbf{B}_u(\mathbf{q},t)\mathbf{u})\end{bmatrix} \tag{17}$$

In this study, the classical explicit fourth-order Runge–Kutta solver is used to compute a fourth-order approximate solution of the equations of motion. This numerical integration scheme can be formulated as follows:

$$\begin{cases}\mathbf{Z}^1=\mathbf{z}_0\\ \mathbf{Z}^{i+1}=\mathbf{RKIV}(\mathbf{Z}^i,\mathbf{U}^i,t^i)\end{cases},\quad i=1,2,\ldots,N \tag{18}$$

being:

$$\mathbf{RKIV}(\mathbf{Z}^i,\mathbf{U}^i,t^i)=\mathbf{Z}^i+\frac{\Delta t}{6}\left(\mathbf{Z}_1^i+2\mathbf{Z}_2^i+2\mathbf{Z}_3^i+\mathbf{Z}_4^i\right),\quad i=1,2,\ldots,N \tag{19}$$

and

$$\begin{cases}\mathbf{Z}_1^i=\mathbf{g}(\mathbf{Z}^i,\mathbf{U}^i,t^i)\\ \mathbf{Z}_2^i=\mathbf{g}(\mathbf{Z}^i+\frac{\mathbf{Z}_1^i}{2},\mathbf{U}^{i+1/2},t^i+\frac{\Delta t}{2})\\ \mathbf{Z}_3^i=\mathbf{g}(\mathbf{Z}^i+\frac{\mathbf{Z}_2^i}{2},\mathbf{U}^{i+1/2},t^i+\frac{\Delta t}{2})\\ \mathbf{Z}_4^i=\mathbf{g}(\mathbf{Z}^i+\mathbf{Z}_3^i,\mathbf{U}^{i+1},t^i+\Delta t)\end{cases},\quad i=1,2,\ldots,N \tag{20}$$

where $\mathbf{Z}^i$ and $\mathbf{U}^i$ represent the approximate and exact discrete versions of the state and input vector $\mathbf{z}$ and $\mathbf{u}$ at the time instant t^i, respectively. Thus, the state-space model provided in Equation (15) can be solved together with relevant initial values using a first-order ordinary differential equation system solver, such as the explicit fourth-order Runge-Kutta numerical integration scheme defined in Equation (18), leading to a discrete set of state-space vectors:

$$\mathbf{Z}=\begin{bmatrix}\mathbf{Z}^1\\ \mathbf{Z}^2\\ \vdots\\ \mathbf{Z}^i\\ \vdots\\ \mathbf{Z}^{l-1}\\ \mathbf{Z}^l\end{bmatrix} \tag{21}$$

where $\mathbf{Z}^i$ refers to the value of the state vector of dimensions $n_z\times 1$ at the discrete-time point t^i and $\mathbf{Z}$ is a column vector of dimensions $ln_z\times 1$.

Although this is not strictly necessary for the computer implementation of the approach devised in this paper, for simplicity, it is assumed herein that the number of states considered in the nonlinear regression $n_{\bar{z}}$ is a subset of the actual number of states n_z and equals the number of inputs n_u, thereby leading to $M=ln_u=ln_{\bar{z}}$. Thus, the output array employed in the regression method is the vector $\mathbf{Y}=\bar{\mathbf{Z}}$, where $\bar{\mathbf{Z}}$ is a column vector of dimensions $ln_{\bar{z}}\times 1$ formed with subsets of the discrete state vector $\bar{\mathbf{Z}}^i$ of dimensions $n_{\bar{z}}\times 1$ corresponding to the discrete-time point t^i.

Operationally, the nonlinear regression analysis can be readily performed by using the `nlinfit` built-in function available in MATLAB. To this end, in addition to the input and output arrays $\mathbf{X}$ and $\mathbf{Y}$, the system model function $\mathbf{f}(\mathbf{X},\mathbf{b})$ and the initial estimate of the vector of unknown system parameters $\mathbf{b}_0$ are also utilized. At the end of the nonlinear regression process, the best values of the unknown parameters, grouped in the vector $\mathbf{b}$, are computed. Then, the relevant state vector components are regenerated using these identified unknown parameters for a final performance evaluation.

4. First Benchmark Problem

In this section, the one-degree-of-freedom nonlinear mechanical system used to test the proposed approach is explained in detail. The nonlinear mechanical system considered as the first benchmark problem is a mass-spring-damper system with Coulomb friction shown in Figure 1.

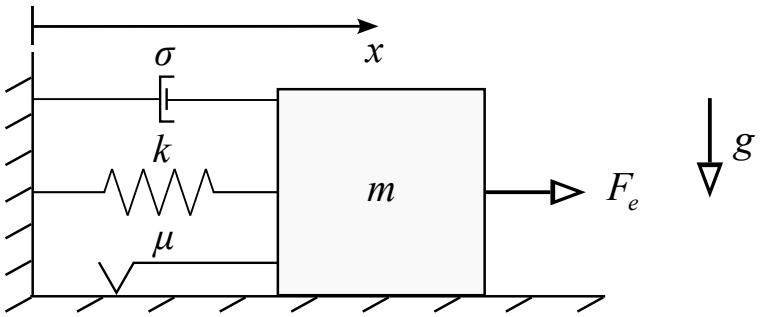

Figure 1. Mass-spring-damper system with Coulomb friction.

The mechanical system shown in Figure 1 is modeled in a Euclidean space of dimension $d = 2$ and has $N_b = 1$ body, except the ground. The body is modeled as a point mass, referred to as the cart. The mobility of the cart is constrained by $N_\Psi = 1$ kinematic joint. To achieve mobility only in the horizontal direction, a prismatic joint is defined between the cart and the ground. Thus, the system degree of freedom is computed as $n_f = 1$.

In Figure 1, a cart of mass m is interconnected through a linear spring having an elastic stiffness coefficient k and a linear damper having a linear damping coefficient σ arranged in parallel. Furthermore, the prismatic joint connecting the cart to the ground allows one degree of freedom of relative translational motion. The constructive and surface imperfections of the prismatic joint introduce an additional resistive force due to dry friction at the mechanical joint, modeled with a constant friction coefficient μ, which induces an external nonconservative mechanical action. The goal of this first demonstrative example is to determine the linear viscous damping coefficient σ and the dry friction coefficient μ associated with a highly nonlinear friction force through the use of the nonlinear identification procedure proposed in this work.

To clarify the schematic diagram of the mass-spring-damper system subjected to dry friction shown in Figure 1, it is worth noting that the cart is depicted in a general configuration with a nonzero displacement x. In particular, the elastic spring, with a stiffness coefficient denoted by k, has a zero undeformed length l_0, meaning the spring only exerts a reaction force when the linear displacement of the cart is different from zero. The spring elongation, $\Delta = l - l_0$, is therefore equal to the cart displacement x, as the current length of the spring l equals the system displacement. This is the principal simplifying assumption used in developing the mechanical model for the first benchmark example.

It is important to note that the simplifying assumptions considered for the mathematical modeling of the first benchmark system, namely the mass-spring-damper system with dry friction, do not affect the quality of the subsequent parameter identification process. This is because the dynamic model of the mass-spring-damper system, deriving from these simplifying assumptions, is used to generate both the reference and estimated dynamic behaviors of the dynamic system of interest, as shown in detail below.

For simplicity, since the minimal coordinate formulation is used, the number of generalized coordinates n_q is equal to the degree of freedom of the entire system n_f. For this benchmark problem, the generalized coordinate is chosen as $x(t)$, which represents the displacement of the cart in the horizontal direction, while t denotes the time variable.

Additionally, the assumed set of initial conditions for the mass-spring-damper system with Coulomb friction is given below:

$$x(0) = x_0, \quad \dot{x}(0) = v_0 \tag{22}$$

where x_0 and v_0 denote, respectively, the initial linear displacement and the initial linear velocity of the cart. Since the cart can only translate in the horizontal direction, the only necessary inertia parameter is the cart mass, which is represented by m.

It is assumed that the system is under the influence of the gravitational acceleration g, which is directed downwards. Furthermore, four force elements are acting on this nonlinear vibrating system. These are a translational spring between the cart and the ground, whose reaction force F_k is proportional to a stiffness coefficient having a constant value k, an external time-dependent force F_e that is exerted on the cart in the horizontal direction, a friction force F_f, characterized by a constant friction coefficient μ, which arises from the interaction between the cart and the ground, and a translational damper located between the cart and ground providing another reaction force F_σ, whose viscous coefficient is designated by a constant value σ.

The external force time law chosen to describe the applied input is defined as $F_e = F_0 u$, where F_0 is the external force amplitude and u represents the external force input function. The external force input function can be defined for the five different scenarios identified as follows:

$$u = \begin{cases} 0, & \text{Case 1 : None} \\ H(t), & \text{Case 2 : Step} \\ \sin(\Omega t), & \text{Case 3 : Harmonic} \\ at, & \text{Case 4 : Linear} \\ \sin(2\pi c t^2), & \text{Case 5 : Chirp} \end{cases} \tag{23}$$

where $H(t)$ refers to the unit step function, also known as the Heaviside step function, defined below:

$$H(t) = \begin{cases} 1, & t \geq 0 \\ 0, & t < 0 \end{cases} \tag{24}$$

In Equation (23), t is the time variable, Ω is the external force angular frequency, a is the external force linear coefficient, and c is the external force chirp rate employed as input. In Equation (24), for simplicity, it is assumed that the initial instant of time used for defining the Heaviside step function is indeed $t_0 = 0$.

On the other hand, one can also define another system property called natural angular frequency, which is defined as $\omega_n = \sqrt{\frac{k}{m}}$, where ω_n represents the natural angular frequency of the linearized system. The damper viscous coefficient can also be written as $\sigma = \xi \sigma_c$, where ξ represents the dimensionless damping factor and σ_c denotes the critical damping coefficient of the linearized system. In particular, the critical damping coefficient is defined as $\sigma_c = 2\sqrt{km}$.

Additionally, the friction force F_f is expressed via the classical Coulomb friction force model, which is given by the following highly nonlinear function:

$$F_f = -\mu W \text{sign}(\dot{x}) \tag{25}$$

where μ denotes the dry friction coefficient between the cart and the ground, $W = mg$ is the cart weight, and $\dot{x}$ represents the linear velocity of the cart.

Under these circumstances, by applying one of the fundamental principles of dynamics, one can write the equation of motion of the mechanical system under study as given below:

$$F_i + F_k + F_\sigma + F_f + F_e = 0 \tag{26}$$

It follows that:

$$-m\ddot{x} - kx - \sigma\dot{x} - \mu W \text{sign}(\dot{x}) + F_0 u = 0 \tag{27}$$

which leads to:

$$\ddot{x} + 2\xi\omega_n\dot{x} + \omega_n^2 x + \mu g \text{sign}(\dot{x}) = f_0 u \tag{28}$$

where $F_i = -m\ddot{x}$ is the inertia force of the cart, $F_k = -kx$ is the elastic force of the spring, $F_\sigma = -\sigma\dot{x}$ is the viscous force of the damper, $F_f = -\mu W \text{sign}(\dot{x})$ is the dissipative force due to friction, $F_e = F_0 u$ is the externally applied force, $\ddot{x}$ represents the acceleration of the cart, and f_0 is the specific applied force amplitude defined as $f_0 = \frac{F_0}{m}$.

Analyzing Equation (28), it is apparent that the dynamic model of the first benchmark system discussed in the paper yields a highly nonlinear second-order ordinary differential equation capable of capturing the complex nonlinear translational vibrations of the cart. It is also important to note that the physical parameters introduced here to describe Equation (28), although identical to those used in a linearized model, are employed to mathematically simplify the resulting analytical expressions of the equations of motion that describe the cart motion. Therefore, no linearization is used throughout this first benchmark example to characterize the cart dynamic behavior.

It should be noted that the governing differential equation given in Equation (28) is nonlinear because of the fourth term on the left-hand side. Thus, its solution can be obtained only by numerically solving the corresponding initial value problem. For that purpose, Equation (28) is converted into the following state-space form:

$$\dot{\mathbf{z}}_c = \mathbf{g}_c(\mathbf{z}_c, u, t) \tag{29}$$

where $n_z = 2n_q = 2$ is the number of states and $\mathbf{z}_c$ refers to the $n_z \times 1$ state vector of the mass-spring-damper system with Coulomb friction defined as:

$$\mathbf{z}_c = \begin{bmatrix} x \\ \dot{x} \end{bmatrix} \tag{30}$$

In Equation (29), $\mathbf{g}_c(\mathbf{z}_c, u, t)$ represents the $n_z \times 1$ state function of the mass-spring-damper system with Coulomb friction, which is expressed as follows:

$$\mathbf{g}_c(\mathbf{z}_c, u, t) = \begin{bmatrix} \dot{x} \\ \ddot{x} \end{bmatrix} = \begin{bmatrix} \dot{x} \\ -\omega_n^2 x - 2\xi\omega_n\dot{x} - \mu g \text{sign}(\dot{x}) + f_0 u \end{bmatrix} \tag{31}$$

The numerical values of the system parameters of the mass-spring-damper system with Coulomb friction are reported in Table 1.

Table 1. Mechanical system model data for the first benchmark problem.

Descriptions	Symbols	Values (Units)
Cart mass	m	5 (kg)
Spring elastic stiffness	k	200 (N/m)
Cart dimensionless damping factor	ξ	0.05 (-)
Cart dry friction coefficient	μ	0.1 (-)
Gravity acceleration	g	9.807 (m/s^2)
Cart initial linear displacement	x_0	0.1 (m)
Cart initial linear velocity	v_0	2 (m/s)
External force amplitude	F_0	100 (N)
External force angular frequency	Ω	3 (rad/s)
External force linear coefficient	a	0.5 (1/s)
External force chirp rate	c	0.2 (1/s)

In the dynamic simulations, the time step is taken as $\Delta t = 10^{-3}$ (s) and the simulation time span is defined as $T_s = 10$ (s).

It is worth noting that the external force amplitude F_0 reported in Table 1 represents the magnitude of the input force used in all the numerical experiments involving the first benchmark system. Meanwhile, the specific time law applied to the input function u varies depending on the case study of the mass-spring-damper system with Coulomb friction, as shown in Equation (23). Therefore, the external force amplitude F_0 is a physical parameter that characterizes the external excitation force $F_e = F_0 u$, regardless of the initial linear displacement of the cart x_0, whose numerical value is also listed in Table 1.

The unknown parameter vector for the dynamic system analyzed herein can be written as follows:

$$\mathbf{b} = \begin{bmatrix} \xi \\ \mu \end{bmatrix} \tag{32}$$

where $n_b = 2$ is the number of unknown parameters of the problem under study contained in the parameter vector $\mathbf{b}$ of dimensions $n_b \times 1$.

The unknown parameters of the nonlinear system under study are estimated using the identification approach devised in this investigation, specifically employing the Levenberg–Marquardt method in conjunction with the Runge–Kutta technique briefly described in Sections 2 and 3. This algorithm is an iterative optimization technique, and the iteration starts with the system parameter vector initial estimation given below:

$$\mathbf{b}_0 = \begin{bmatrix} \xi_0 \\ \mu_0 \end{bmatrix} \tag{33}$$

where ξ_0 and μ_0 are defined as follows:

$$\xi_0 = \left(1 + \frac{\epsilon}{100}\right)\xi, \quad \mu_0 = \left(1 + \frac{\epsilon}{100}\right)\mu \tag{34}$$

where ξ_0 represents the initial estimation of the dimensionless damping factor, μ_0 refers to the initial estimation of the dry friction coefficient, and ϵ denotes an initial estimation relative error, which is artificially introduced in the initial guess for the system parameter estimation to test the effectiveness of the approach devised in this paper. In conclusion, Table 2 illustrates the parameters used in the nonlinear estimation process proposed in this paper, which is applied to the first benchmark system.

Table 2. Numerical values of the parameters used in the nonlinear estimation process for the first benchmark problem.

Descriptions	Symbols	Values (Units)
Initial estimation relative error	ϵ	200 (%)
Cart dimensionless damping factor initial estimation	ξ_0	0.15 (-)
Cart dry friction coefficient initial estimation	μ_0	0.3 (-)

5. Second Benchmark Problem

In the second benchmark problem, a simple pendulum-damper system with Coulomb friction is considered to evaluate the approach proposed in this study, as shown in Figure 2. The nonlinear parameter identification of this second benchmark problem is more challenging than that of the first because the 'degree of nonlinearity' is higher than in the previous benchmark problem. This is because of the intrinsic geometric nonlinearity that characterizes the simple pendulum system.

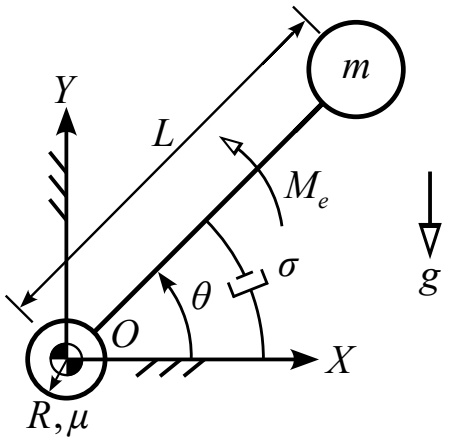

Figure 2. Simple pendulum-damper system with Coulomb friction.

The modeling space considered for the system represented in Figure 2 is a Euclidean space of dimension $d = 2$, and the mechanical system consists of $N_b = 1$ body, which is modeled here as a point mass, excluding ground. The point mass is connected to the point O via a massless rod of length L. Its motion is constrained via $N_\Psi = 1$ kinematic joint. A revolute joint, which is collocated at point O and is defined between the massless rod and the ground, is used for that purpose. Therefore, the degree of freedom of the mechanical system is simply computed as $n_f = 1$.

In Figure 2, a bob of mass m is interconnected to the ground through a massless rod of length L to form a simple pendulum, while an angular dashpot having a viscous damping coefficient σ is collocated between the massless rod and the horizontal axis of the ground. Thus, the revolute joint connecting the massless rod to the ground provides one degree of relative rotational freedom. Since the pendulum undergoes large finite rotations, the presence of the vertical gravity force associated with the constant acceleration g induces significant geometric nonlinearities in the mechanical model of the simple pendulum system under study. Additionally, the constructive and surface imperfections of the revolute joint introduce an additional resistive force due to dry friction at the mechanical joint, modeled with a constant friction coefficient μ, which induces an external nonconservative mechanical action. The goal of this second demonstrative example is to determine the angular viscous damping coefficient σ and the dry friction coefficient μ associated with a highly nonlinear friction moment through the use of the nonlinear identification procedure proposed in this work.

To clarify the schematic diagram of the simple pendulum system shown in Figure 2, it is worth noting that the size of the revolute joint located at point O is enlarged in this figure. This helps visually explain the meaning of the pivot radius R and the dry friction coefficient μ between the cylindrical surfaces forming the revolute joint kinematic pairs. Furthermore, for simplicity, in the computation of the closure force necessary for evaluating the dry friction force F_f and its corresponding mechanical moment M_f, the entire pendulum weight W is considered, and the radius R is directly employed for determining the moment arm. This is the main simplifying assumption used in developing the mechanical model for the second benchmark example.

It is worth noting that the simplifying assumptions used in the mathematical modeling of the second benchmark system, specifically the simple pendulum-damper system with dry friction, do not impact the quality of the subsequent parameter identification process. This is because the dynamic model of the pendulum-damper system, based on these simplifying assumptions, is employed to generate both the reference and estimated dynamic behaviors of the system of interest, as explained in detail below.

By adopting the minimal coordinate formulation approach, only $n_q = n_f = 1$ generalized coordinate is used to describe the mechanical system at any instant. The pendulum angular displacement represented by the Lagrangian coordinate $\theta(t)$ is used to this end, while t represents time. Moreover, the set of initial conditions assumed for the simple pendulum-damper system with Coulomb friction can be defined as follows:

$$\theta(0) = \theta_0, \quad \dot{\theta}(0) = \omega_0 \tag{35}$$

where θ_0 and ω_0 denote, respectively, the initial angular displacement and the initial angular velocity of the pendulum. As a result of using a revolute joint at point O, the point mass undergoes a rotational motion around the Z-axis passing by point O. The mass of the particle forming the pendulum is represented by m, as mentioned before. In the mechanical model of the simple pendulum-damper system with Coulomb friction, it is assumed that the pendulum is subjected to the gravitational acceleration g that acts in the negative direction of the Y axis.

There are three force elements in the system, namely an external mechanical moment M_e, a friction torque M_f that arises from the frictional interaction between the pendulum and ground, and a rotational damper that produces a viscous torque M_σ. The external mechanical moment can be expressed as $M_e = M_0 u$, where M_0 refers to the external torque amplitude and u designates the external torque input function. Similar to the first benchmark problem explained in Section 4, five various scenarios, introduced in Equation (23), are assumed for the external torque input function. Additionally, it is assumed that the revolute joint is not ideal and introduces joint friction. To model the joint friction, the classical Coulomb friction force model is used as given below:

$$M_f = -\mu W R \text{sign}(\dot{\theta}) \tag{36}$$

where $W = mg$ is the pendulum weight, M_f refers to the friction mechanical moment, μ stands for the dry friction coefficient, R represents the revolute joint radius, and $\dot{\theta}$ is the angular velocity of the pendulum. The rotational damper, which has a viscous coefficient σ representing a constant value, is also defined between the pendulum and the ground.

For convenience, the following definitions are considered:

$$k_e = mgL, \quad I_e = mL^2 \tag{37}$$

where k_e and I_e respectively represent the equivalent stiffness coefficient and the equivalent mass moment of inertia of the simple pendulum. Based on these definitions, the natural angular frequency of the linearized system is defined as $\omega_n = \sqrt{\frac{k_e}{I_e}}$. Furthermore, the viscous coefficient σ is also given by $\sigma = \xi \sigma_c$, where ξ refers to the dimensionless damping factor and σ_c represents the critical damping coefficient of the linearized system model, which can be defined as $\sigma_c = 2\sqrt{k_e I_e}$. Thus, the equation of motion of the simple pendulum subjected to dry friction can be mathematically written as follows:

$$M_i + M_g + M_\sigma + M_f + M_e = 0 \tag{38}$$

It follows that:

$$-I_e \ddot{\theta} - k_e \cos(\theta) - \sigma \dot{\theta} - \mu W R \text{sign}(\dot{\theta}) + M_0 u = 0 \tag{39}$$

which leads to:

$$\ddot{\theta} + 2\xi\omega_n \dot{\theta} + \omega_n^2 \cos(\theta) + \mu \omega_n^2 \eta \text{sign}(\dot{\theta}) = A_0 u \tag{40}$$

where $M_i = -I_e\ddot{\theta}$ is the inertia mechanical moment of the pendulum, $M_g = -k_e\cos(\theta)$ is the conservative mechanical moment due to gravity, $M_\sigma = -\sigma\dot{\theta}$ is the viscous mechanical moment of the damper, $M_f = -\mu WR\text{sign}(\dot{\theta})$ is the dissipative mechanical moment due to friction, $M_e = M_0 u$ is the externally applied mechanical moment, and $\ddot{\theta}$ represents the angular acceleration of the pendulum. Additionally, η and A_0 respectively refer to the geometric dimension ratio and the external torque specific amplitude, both of which can be defined as given below:

$$\eta = \frac{R}{L}, \quad A_0 = \frac{M_0}{I_e} \tag{41}$$

being the parameters η and A_0 introduced here, defined for the convenience of the mathematical representation of the dynamic model.

Observing Equation (40), it is clear that the dynamic model of the second benchmark system discussed in the paper yields a highly nonlinear second-order ordinary differential equation capable of capturing the complex nonlinear rotational vibrations of the pendulum. It is also noteworthy to point out that the physical parameters introduced here to describe Equation (40), although identical to those used in a linearized model, are employed to mathematically simplify the resulting analytical expressions of the equations of motion that describe the pendulum motion. Therefore, no linearization is employed throughout this second benchmark example to characterize the pendulum dynamic behavior.

It is noteworthy that Equation (40) is highly nonlinear because of the third and fourth terms on the left-hand side, so its solution must be obtained numerically. To this end, Equation (40), which is developed in the configuration space, needs to be rewritten in the state space as given below:

$$\dot{\mathbf{z}}_p = \mathbf{g}_p(\mathbf{z}_p, u, t) \tag{42}$$

In this second benchmark problem, $n_q = 2n_q = 2$ is the number of states and the $n_z \times 1$ state vector $\mathbf{z}_p$ of the simple pendulum-damper system with Coulomb friction can be defined as follows:

$$\mathbf{z}_p = \begin{bmatrix} \theta \\ \dot{\theta} \end{bmatrix} \tag{43}$$

Also, the term $\mathbf{g}_p(\mathbf{z}_p, u, t)$ reported in Equation (42) represents the state function of the simple pendulum-damper system with Coulomb friction defined as:

$$\mathbf{g}_p(\mathbf{z}_p, u, t) = \begin{bmatrix} \dot{\theta} \\ \ddot{\theta} \end{bmatrix} = \begin{bmatrix} \dot{\theta} \\ -\omega_n^2\cos(\theta) - 2\xi\omega_n\dot{\theta} - \mu\omega_n^2\eta\text{sign}(\dot{\theta}) + A_0 u \end{bmatrix} \tag{44}$$

Table 3 presents numerical values of the system parameters of the simple pendulum-damper system with Coulomb friction.

In the computer simulations, the time step is taken as $\Delta t = 10^{-3}$ (s) and $T_s = 10$ (s) represents the simulation time span.

It is important to note that the external torque amplitude M_0 provided in Table 3 represents the magnitude of the input torque employed in all the numerical experiments involving the second benchmark system. Conversely, the particular time law considered for the input function u varies depending on the case study of the simple pendulum-damper system with Coulomb friction, as shown in Equation (23). Thus, the external torque amplitude M_0 is a physical parameter that defines the external excitation torque $M_e = M_0 u$, regardless of the initial angular displacement of the pendulum θ_0, whose numerical value is also included in Table 3.

Table 3. Mechanical system model data for the second benchmark problem.

Descriptions	Symbols	Values (Units)
Pendulum length	L	0.5 (m)
Revolute joint radius	R	0.02 (m)
System geometric dimensions ratio	η	0.04 (-)
Pendulum mass	m	10 (kg)
Gravity acceleration	g	9.807 (m/s^2)
Pendulum dimensionless damping factor	ξ	0.1 (-)
Pendulum dry friction coefficient	μ	0.5 (-)
Pendulum initial angular displacement	θ_0	$\pi/4$ (rad)
Pendulum initial angular velocity	ω_0	1.5 (rad/s)
External torque amplitude	M_0	20 (N $\times$ m)
External torque angular frequency	Ω	5 (rad/s)
External torque linear coefficient	a	0.2 (1/s)
External torque chirp rate	c	0.1 (1/s)

In analogy with the first benchmark problem, the dimensionless damping factor and dry friction parameters are assumed unknowns, so the system unknown parameter vector introduced in Equation (32) is also built in this benchmark problem. Additionally, the system parameter initial estimation vector, as given in Equation (33) and its component definitions in Equation (34), are also valid for this benchmark problem. In conclusion, Table 4 presents the parameters input to the nonlinear estimation process proposed in this paper, which is applied to the second benchmark system.

Table 4. Numerical values of the parameters used in the nonlinear estimation process for the second benchmark problem.

Descriptions	Symbols	Values (Units)
Initial estimation relative error	ϵ	100 (%)
Pendulum dimensionless damping factor initial estimation	ξ_0	0.2 (-)
Pendulum dry friction coefficient initial estimation	μ_0	1 (-)

6. Results and Discussion

6.1. Descriptions of the Numerical Experiments

In this section, the numerical results obtained from both benchmark problems are presented, along with a general discussion of the methodology used to quantify system performance. In the identification process, the displacement signals are utilized to estimate the unknown system parameters through a fitting process. In contrast, the velocity signals are used to validate the accuracy and reliability of the estimated parameters. In all the numerical experiments described herein, five different scenarios are considered for defining the input vector as shown in Equation (23), namely the 'None' input (Case 1), the 'Step' input (Case 2), the 'Harmonic' input (Case 3), the 'Linear' input (Case 4), and the 'Chirp' input (Case 5). This is done for both benchmark problems examined in this paper to verify the effectiveness of the nonlinear identification process devised in this investigation under different operational conditions of practical interest.

At this stage, it is also worth spending a few additional words on the choice of the five forcing functions described in Equation (23). In system identification and experimental modal analysis of structural and mechanical systems, several well-established types of input forcing functions are commonly used [83–85]. For instance, impulse excitation, usually applied with an instrumented hammer, provides a simple way to quickly obtain broadband

information. Random excitation is widely used with shakers because it simultaneously excites many modes and enables effective averaging in frequency response estimation. Sine-based inputs are also fundamental, as stepped-sine testing provides a high signal-to-noise ratio and accurate modal parameter estimation. In particular, swept-sine or chirp excitation provides a continuous frequency sweep, well-suited for large structures that require sustained energy. These excitation types together form the standard toolkit for both linear and nonlinear system identification, each offering a unique balance of energy content, frequency coverage, signal quality, and practicality based on the testing scenario. In this vein, the five different forcing functions reported in Equation (23) were selected for this investigation to assess through numerical experiments the performance of the identification procedure developed in the present paper.

A special comment is necessary for the type of external excitation function considered in Case 4 of Equation (23). First, the linear input force in Case 4 of Equation (23) induces large displacements over a short time frame, thereby enabling a realistic dynamical simulation resulting from progressive loading. Second, the goal of the present numerical experiment is to verify the performance of the proposed method in the presence of significant finite vibrations, and the input force in Case 4 of Equation (23) serves this purpose. Additionally, in experimental modal analysis of structural systems, periodic ramps or sawtooth excitations, similar to the input time history employed in Case 4 of Equation (23) of the present study, are often used because they offer several advantages. Their rich harmonic content provides broadband excitation, enabling many modes to be simultaneously stimulated in a controlled, repeatable manner. Since the waveform is deterministic and periodic, cycle averaging enhances signal-to-noise ratios and enables the precise extraction of harmonic responses for estimating the frequency content of linear dynamical systems. The harmonic spectrum, in this case, also provides strong high-frequency content, which is more effective than impact excitation for identifying higher modes of structural systems. Furthermore, since the waveform partially resembles the classical shock pulses, it helps validate modal models of flexible structures under realistic transient loads. For these reasons, a linearly growing time law for the input excitation was adopted in Case 4 of Equation (23) for numerical experiments.

To achieve the goal of identifying the physical parameters of interest for this study, in the computer implementation of the nonlinear identification procedure proposed in this work, a MATLAB function was created to compute the system state vector given in Equation (21) using the constant-step-size fourth-order Runge–Kutta method described by Equations (18)–(20), with the unknown parameter vector of Equation (32) and the external excitation functions shown in Equation (23) as functional inputs reshaped in the input vector of Equation (14). By doing so, one can readily define another MATLAB function that implements the nonlinear function describing the system model of interest reported in Equation (1), thereby facilitating the subsequent computer implementation of the Levenberg–Marquardt nonlinear regression algorithm employed in this paper. Thus, all the identified numerical results presented in this section are based on the MATLAB implementation of the computational approach described above and discussed in detail in Sections 2 and 3.

In the numerical experiments carried out for the first and second benchmark systems considered in the paper, a comparison is made between the original numerical results coming from dynamic simulations performed using the original reference values of the unknown parameters with those obtained from the identified physical parameters, namely the dashpot dimensionless damping factor ξ and the dry friction coefficient μ that appear in the dynamical models of the cart and of the pendulum described by Equations (31) and (44). This was done to qualitatively and quantitatively compare the performance of the iterative identification process developed in this paper and to assess its effects on the vibrational behavior of the dynamic systems under study. Therefore, throughout the results of the

dynamical simulations reported below, it is assumed that the identification procedure proposed in this paper was run in advance to obtain the numerical values of the unknown physical parameters to include in the parameter vector of Equation (32).

6.2. Numerical Results of the First Benchmark Problem

This subsection presents the numerical results obtained for the first benchmark problem, the mass-spring-damper system with the presence of Coulomb friction explained in Section 4, for the five external force input functions considered in this study.

Figure 3 shows the numerical vibration responses of the nonlinear mechanical system and the identified vibration signals with the identified unknown parameters in the absence of any input function.

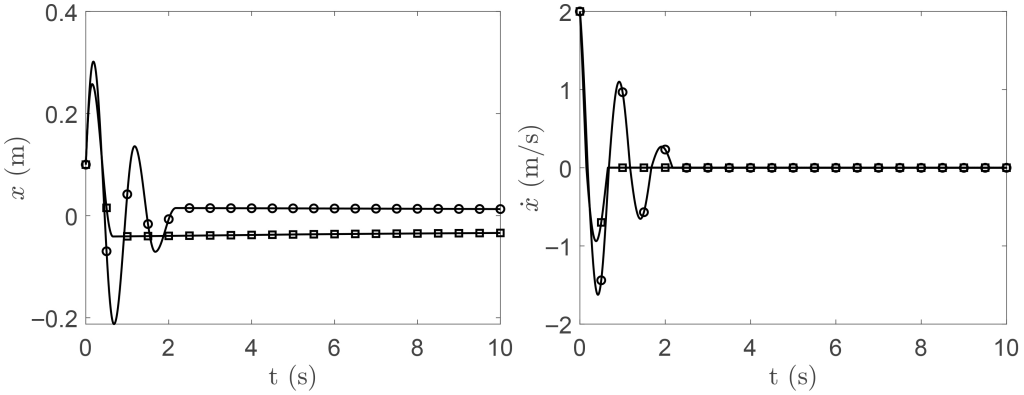

(**a**) (**b**)

Figure 3. Vibration responses of the first benchmark problem for the zero input force of Case 1 (○: Numerical results, □: Identified results). (**a**) Linear displacement. (**b**) Linear velocity.

In particular, Figure 3a shows the displacement signals, whereas Figure 3b shows the velocity signals in Case 1 of the mass-spring-damper system with dry friction. As can be seen from the dynamic simulation results presented in Figure 3, in the absence of any external excitation force, the system first vibrates due to the initial conditions, and over time, the amplitude of this motion decreases due to the presence of the translational damper and the Coulomb friction, thereby reaching zero approximately after two seconds. On the other hand, the identification algorithm cannot detect this initial vibration phase and converges to a nonzero displacement value after approximately one second.

A similar behavior can also be observed in Figure 4 for the step input force.

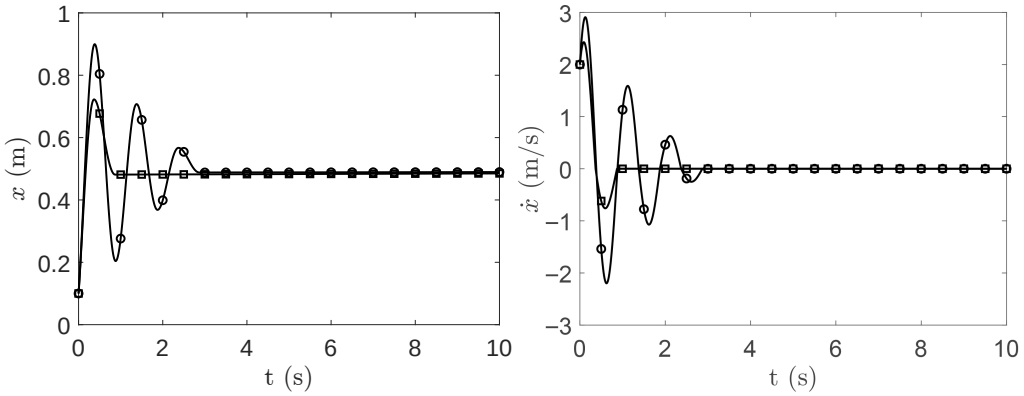

(**a**) (**b**)

Figure 4. Vibration responses of the first benchmark problem for the step input force of Case 2 (○: Numerical results, □: Identified results). (**a**) Linear displacement. (**b**) Linear velocity.

Figure 4a shows the displacement signals, while Figure 4b represents the velocity signals in Case 2 of the mass-spring-damper system with dry friction. One can see from Figure 4 that, after an initial vibrational phase, the system oscillations are damped out around a nonzero value due to the step input force. On the other hand, the identification algorithm cannot estimate the initial vibrational phase correctly while converging on the correct value.

For the harmonic input force, the dynamic simulation results and the identified system responses are presented in Figure 5.

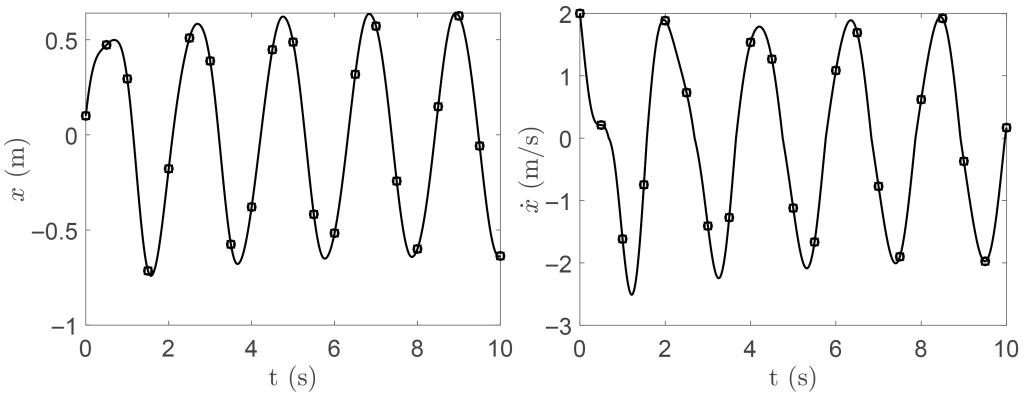

(**a**) (**b**)

Figure 5. Vibration responses of the first benchmark problem for the harmonic input force of Case 3 (○: Numerical results, □: Identified results). (**a**) Linear displacement. (**b**) Linear velocity.

Figure 5a shows the displacement signals, while Figure 5b illustrates the velocity signals in Case 3 of the mass-spring-damper system with dry friction. It is apparent from Figure 5 that the identified displacement and velocity signals are successfully matched with the numerical signals for the harmonic input force.

For the linear input force, the dynamic simulation results and identified system responses are compared in Figure 6.

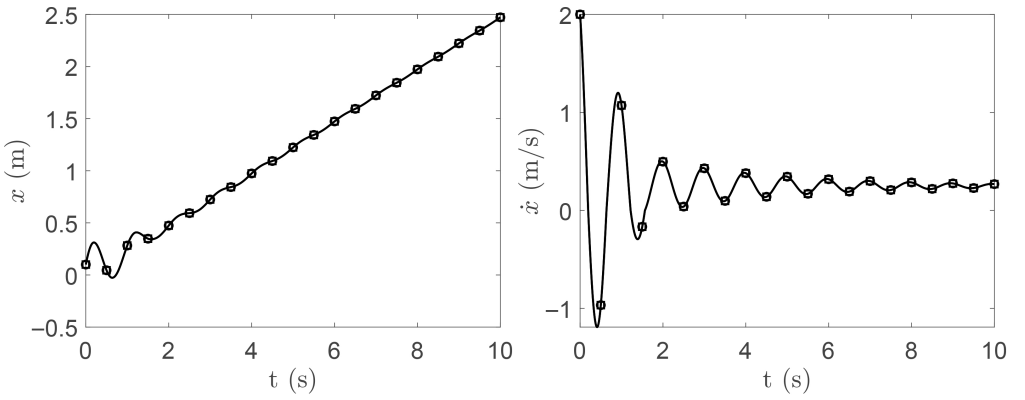

(**a**) (**b**)

Figure 6. Vibration responses of the first benchmark problem for the linear input force of Case 4 (○: Numerical results, □: Identified results). (**a**) Linear displacement. (**b**) Linear velocity.

Figure 6a shows the displacement signals, while Figure 6b represents the velocity signals in Case 4 of the mass-spring-damper system with dry friction. As shown in Figure 6, the identification algorithm can successfully estimate the output response for the linear input force scenario.

Figure 7 shows the dynamic simulation results and the identified vibration signals for the chirp input function.

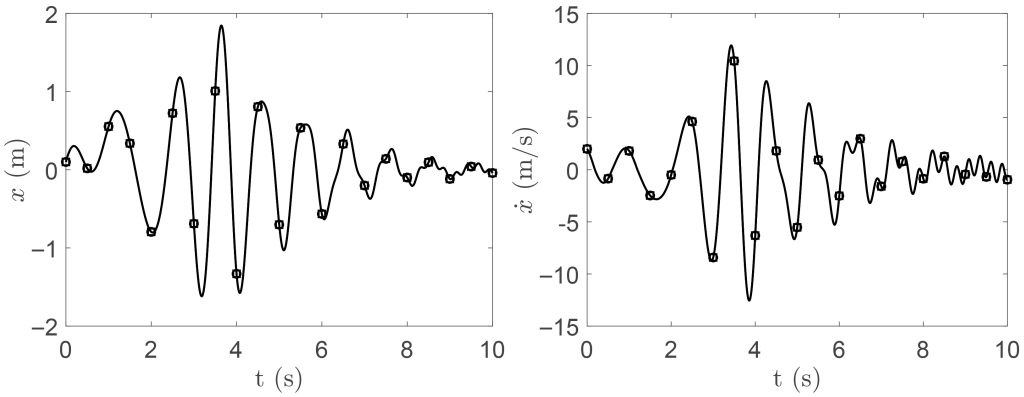

(**a**) (**b**)

Figure 7. Vibration responses of the first benchmark problem for the chirp input force of Case 5 (○: Numerical results, □: Identified results). (**a**) Linear displacement. (**b**) Linear velocity.

Figure 7a shows the displacement signals, while Figure 7b illustrates the velocity signals in Case 5 of the mass-spring-damper system with dry friction. Figure 7 demonstrates that the identified displacement and velocity signals align closely with the dynamic simulation results, indicating a successful match between the simulated and identified data.

6.3. Numerical Results of the Second Benchmark Problem

This subsection reports the numerical results obtained from the dynamic simulations and identification process for the second benchmark problem, which is a simple pendulum-damper system with Coulomb friction explained in Section 5, for the five external torque input functions considered in this investigation.

The dynamic simulation results and estimated system dynamic responses are presented in Figure 8 in the absence of any input torque.

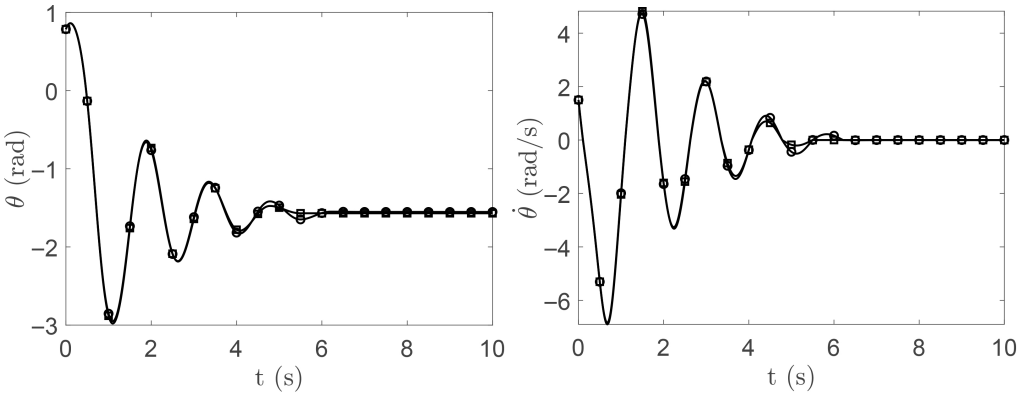

(**a**) (**b**)

Figure 8. Vibration responses of the second benchmark problem for the zero input torque of Case 1 (○: Numerical results, □: Identified results). (**a**) Angular displacement. (**b**) Angular velocity.

In particular, Figure 8a shows the displacement signals, whereas Figure 8b illustrates the velocity signals in Case 1 of the simple pendulum-damper system with Coulomb friction. From Figure 8, one can infer that the identified system responses are generally in good agreement with the dynamic simulation results except for a few points, especially between the fourth and sixth seconds. It can be said that for this input torque scenario, the

agreement between the dynamic simulation results and the identified system responses is at a better level than the first benchmark problem.

The comparison of dynamic simulation results and the identified system responses for the step input torque is presented in Figure 9.

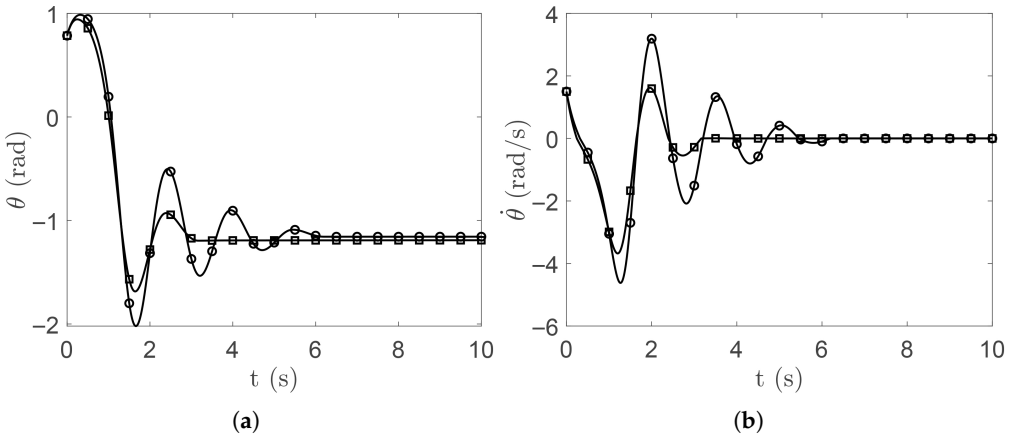

(**a**) (**b**)

Figure 9. Vibration responses of the second benchmark problem for the step input torque of Case 2 (○: Numerical results, □: Identified results). (**a**) Angular displacement. (**b**) Angular velocity.

Figure 9a shows the displacement signals, while Figure 9b illustrates the velocity signals in Case 2 of the simple pendulum-damper system with Coulomb friction. From Figure 9, it is evident that the identification algorithm cannot accurately estimate the actual system behavior, as obtained from the dynamic simulation, although the estimation is improved compared to the first benchmark problem for this input torque scenario.

The comparison of dynamic simulation results and identified system response is presented in Figure 10 for the harmonic input torque.

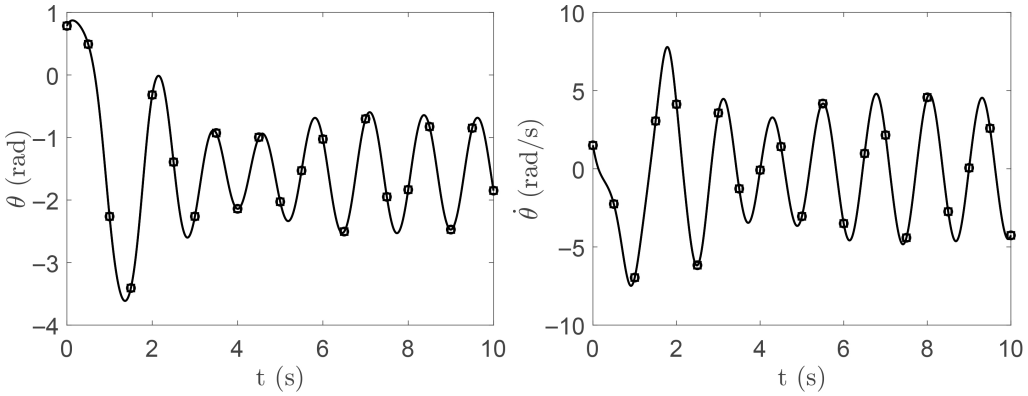

(**a**) (**b**)

Figure 10. Vibration responses of the second benchmark problem for the harmonic input torque of Case 3 (○: Numerical results, □: Identified results). (**a**) Angular displacement. (**b**) Angular velocity.

Figure 10a reports the displacement signals, while Figure 10b provides the velocity signals in Case 3 of the simple pendulum-damper system with Coulomb friction. Figure 10 demonstrates that the identified displacement and velocity signals align closely with the dynamic simulation results, indicating a successful match between the identified and dynamic simulation data.

Figure 11 provides the dynamic simulation results and the identified system responses for the linear input torque case.

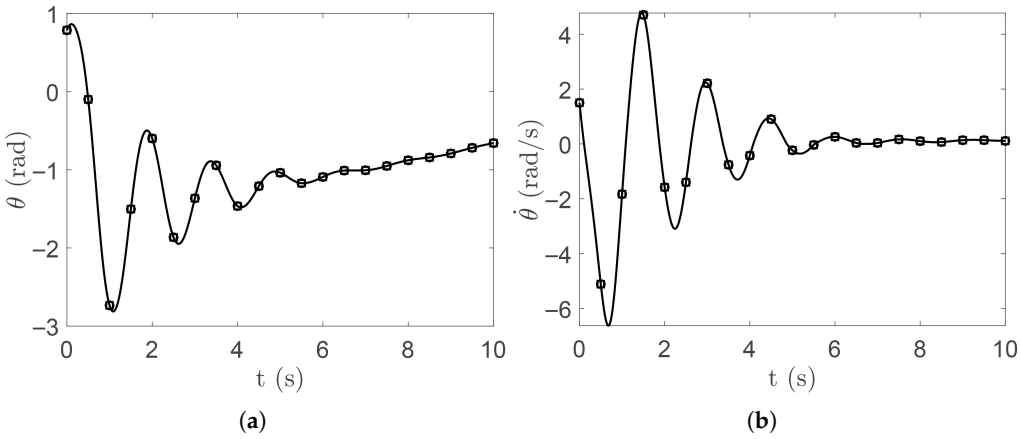

(**a**) (**b**)

Figure 11. Vibration responses of the second benchmark problem for the linear input torque of Case 4 (○: Numerical results, □: Identified results). (**a**) Angular displacement. (**b**) Angular velocity.

While Figure 11a presents the displacement signals, Figure 11b shows the velocity signals in Case 4 of the simple pendulum-damper system with Coulomb friction. As can be seen from Figure 11, dynamic simulation results and identified system responses are in very good agreement, similar to the first benchmark problem.

The comparison of dynamic simulation results and identified system responses for the chirp input torque scenario is illustrated in Figure 12.

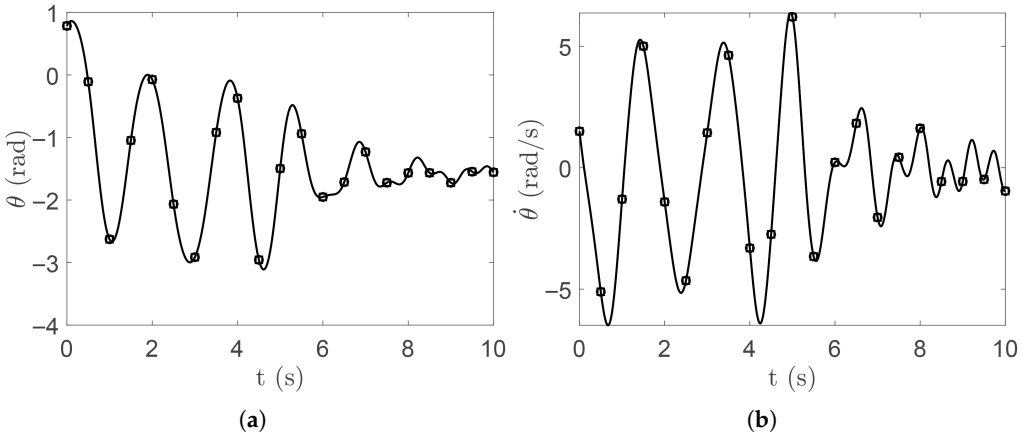

(**a**) (**b**)

Figure 12. Vibration responses of the second benchmark problem for the chirp input torque of Case 5 (○: Numerical results, □: Identified results). (**a**) Angular displacement. (**b**) Angular velocity.

Figure 12a reports the displacement signals, while Figure 12b represents the velocity signals in Case 5 of the simple pendulum-damper system with Coulomb friction. Figure 12 indicates that the identified displacement and velocity signals align closely with the signals obtained from the dynamic simulation, indicating a successful match between the identified and dynamic simulation data.

6.4. General Discussion

In this study, extensive dynamical simulations are carried out by employing two mechanical models for the two benchmark systems considered in the paper. These are: (a) a first mechanical model based on the actual numerical values of the parameter vector $\mathbf{b}$; (b) a second mechanical model based on an estimation of the numerical values of the parameter vector $\hat{\mathbf{b}}$. In the first mechanical model, the set of numerical values for the system parameter vector $\mathbf{b}$ is kept constant across all simulation scenarios, using the default values reported in Tables 1 and 3, respectively, for the two demonstrative examples. In the second mechanical

model, on the other hand, the numerical values used to estimate the actual parameter vector $\mathbf{b}$ are updated iteratively starting from the initial guess $\mathbf{b}_0$, respectively shown in Tables 2 and 4, thereby trying to gradually improve the current estimation of the parameter vector denoted by $\hat{\mathbf{b}}$. When the nonlinear regression method described in the paper works correctly, the estimated parameter vector $\hat{\mathbf{b}}$ converges to the actual parameter vector $\mathbf{b}$. If this is the case, the estimated time laws of the system generalized coordinates must overlap the reference ones. Otherwise, the estimation of the parameter vector $\hat{\mathbf{b}}$ cannot precisely identify the desired set of unknown parameters $\mathbf{b}$.

In Figures 3–12, the numerical results displayed with the circle markers are obtained using the actual value of the system parameter vector $\mathbf{b}$, while the identified results displayed with the square markers are obtained using the best estimated value of the system parameter vector $\hat{\mathbf{b}}$. Thus, in Figures 3–12, the numerical results represented with circle markers are the reference time laws for both benchmark systems, whereas the identified results represented with square markers are the corresponding estimated time laws. Consequently, the quantitative criterion employed in this investigation to assess the quality of the identified results is a function of the difference between the actual and estimated parameter vectors $\mathbf{b}$ and $\hat{\mathbf{b}}$ considered for both benchmark systems, as well as its impact in the resulting time laws of the generalized coordinates describing the two demonstrative examples analyzed in this study.

For the reasons thoroughly discussed above, this subsection is devoted to evaluating the effectiveness of the identification process of the damping factor ξ and the dry friction coefficient μ for both benchmark problems considered in the paper. To this end, two error metrics, namely the relative error and the root-mean-square error, are used.

The relative errors are computed as given below for both parameters:

$$\text{error}(\xi) = \frac{|\hat{\xi} - \xi|}{\xi}, \quad \text{error}(\mu) = \frac{|\hat{\mu} - \mu|}{\mu} \tag{45}$$

where $\text{error}(\xi)$ and $\text{error}(\mu)$ are respectively the relative error for the dimensionless damping factor and the relative error for the dry friction coefficient. Additionally, while $\hat{\xi}$ and $\hat{\mu}$ respectively refer to the identified dimensionless damping factor and the identified dry friction coefficient, the parameters ξ and μ respectively denote the actual correct values of the dimensionless damping factor and the dry friction coefficient used to numerically generate the reference measurements employed in the nonlinear identification process.

The root-mean-square error is also defined as follows:

$$\text{RMSE}(y) = \sqrt{\sum_{i=1}^{N} \frac{(\hat{y}_i - y_i)^2}{N}} \tag{46}$$

where $\text{RMSE}(y)$ is the root-mean-square error of the relevant state, while $\hat{y}_i$ and y_i respectively refer to ith components of the identified state and the reference state.

Table 5 presents the identified unknown parameters, the computed relative errors of them, and the root-mean-square errors calculated for the cart linear displacement x and the cart linear velocity $\dot{x}$ for the five input functions. As can be seen from Table 5, the identification algorithm is unable to estimate the exact values of the dimensionless damping factor and dry friction coefficient for both zero-input force (Case 1) and step-input force (Case 2) scenarios. On the other hand, in the scenarios that separately include the harmonic, linear, and chirp input forces (Cases 3, 4, and 5), the identification algorithm can accurately estimate unknown parameters. In effect, very good agreement is observed for the harmonic, linear, and chirp input force scenarios, which are consistent with the time histories obtained through the dynamical simulations shown in Figures 5–7.

Table 5. Numerical results of the nonlinear regression used for the parametric identification of the first benchmark problem.

Symbolic Quantity	Numerical Values	None Input Identified Values	Step Input Identified Values	Harmonic Input Identified Values	Linear Input Identified Values	Chirp Input Identified Values
ξ	5.000×10^{-2}	1.500×10^{-1}	1.492×10^{-1}	5.000×10^{-2}	5.000×10^{-2}	5.000×10^{-2}
μ	1.000×10^{-1}	3.000×10^{-1}	3.010×10^{-1}	1.000×10^{-1}	1.000×10^{-1}	1.000×10^{-1}
error(ξ)	-	2.000×10^{0}	1.985×10^{0}	2.637×10^{-15}	1.334×10^{-13}	2.498×10^{-15}
error(μ)	-	2.000×10^{0}	2.010×10^{0}	1.527×10^{-15}	5.829×10^{-14}	1.943×10^{-14}
RMSE(x)	-	6.113×10^{-2}	6.825×10^{-2}	1.505×10^{-16}	1.796×10^{-15}	1.818×10^{-15}
RMSE($\dot{x}$)	-	2.395×10^{-1}	4.057×10^{-1}	9.230×10^{-16}	9.959×10^{-15}	1.130×10^{-14}

The identified unknown parameters, their relative errors, and the root-mean-square errors computed for the pendulum angular displacement θ and the pendulum angular velocity $\dot{\theta}$ for the five input functions are given in Table 6. It is seen from Table 6 that the estimated values for the dimensionless damping factor and the dry friction coefficient exhibit a high degree of accuracy and consistency for the harmonic, linear, and chirp input functions (Cases 3, 4, and 5), while both the zero-input force (Case 1) and step-input force (Case 2) scenarios do not perform well. These results are consistent with the time histories obtained through the dynamical simulations shown in Figures 10–12.

Table 6. Numerical results of the nonlinear regression used for the parametric identification of the second benchmark problem.

Symbolic Quantity	Numerical Values	None Input Identified Values	Step Input Identified Values	Harmonic Input Identified Values	Linear Input Identified Values	Chirp Input Identified Values
ξ	1.000×10^{-1}	8.559×10^{-2}	1.992×10^{-1}	1.000×10^{-1}	1.000×10^{-1}	1.000×10^{-1}
μ	5.000×10^{-1}	1.047×10^{0}	9.879×10^{-1}	5.000×10^{-1}	5.001×10^{-1}	5.000×10^{-1}
error(ξ)	-	1.441×10^{-1}	9.925×10^{-1}	4.996×10^{-15}	1.731×10^{-5}	1.332×10^{-14}
error(μ)	-	1.094×10^{0}	9.758×10^{-1}	8.016×10^{-14}	1.039×10^{-4}	5.596×10^{-14}
RMSE(θ)	-	2.642×10^{-2}	1.496×10^{-1}	2.033×10^{-15}	3.669×10^{-6}	8.055×10^{-15}
RMSE($\dot{\theta}$)	-	9.162×10^{-2}	5.848×10^{-1}	8.928×10^{-15}	1.938×10^{-5}	3.056×10^{-14}

Table 7 contains the computational cost and convergence times for each case study, thereby allowing comparison of these variables across the five scenarios analyzed in this study. In particular, the dimensionless computational times for the nonlinear regression used in the parametric identification of the benchmark problems are shown in Table 7. To ensure a consistent comparison, the simulation times listed in Table 7 are made dimensionless by using the computer time of the dynamical simulation performed in the first scenario with zero-input force (Case 1) of each demonstrative example as a reference.

Table 7. Dimensionless computational times of the nonlinear regression for the parametric identification of the benchmark problems.

	None Input Computer Time	Step Input Computer Time	Harmonic Input Computer Time	Linear Input Computer Time	Chirp Input Computer Time
First Benchmark Problem	1.000	1.261	0.7876	0.9461	1.132
Second Benchmark Problem	1.000	1.041	1.401	9.048	2.262

By examining the convergence times reported in Table 7, it is clear that the most efficient scenario is based on the harmonic input function (Cases 3) for each benchmark system.

Therefore, it can be concluded that, while the harmonic, linear, and chirp input functions (Cases 3, 4, and 5) lead to an effective outcome of the system identification procedure devised in this work, the most efficient scenario for both benchmark problems is based on the harmonic forcing function (Case 3).

As a conclusive remark, it is noted that the absence of any excitation input or the presence of a step input is not efficient in the nonlinear parameter identification process in general. It is observed that an input that leads to sufficiently variable behavior is critical for the success of the identification algorithm. This is because, otherwise, the nonlinear dynamic behavior of the mechanical system of interest is not thoroughly excited and, therefore, captured from the computer simulations or the experimental measurements.

The analysis of both benchmark systems presented in the paper shows that, in scenarios that include the harmonic, linear, and chirp input forces/torques considered separately (Cases 3, 4, and 5), the identification algorithm can reliably estimate unknown damping factor and friction parameter. However, the proposed identification algorithm cannot accurately estimate the exact values of the dimensionless damping factor and dry friction coefficient in both the zero-input force/torque (Case 1) and step-input force/torque (Case 2) scenarios. Consequently, it is evident that the absence of any excitation input or the presence of only a step input generally does not facilitate effective nonlinear parameter identification. Thus, sufficiently variable input behavior is crucial for the success of the proposed identification algorithm, as without it the complex nonlinear dynamics of the mechanical systems under study are not thoroughly excited and, therefore, not adequately captured in the dynamical analysis.

As a final note, it is important to highlight that the numerical experiments conducted in this study show that, although the initial guess for the unknown parameters can be quite rough, the success of the identification process heavily depends on the richness of the external excitation, which may or may not fully solicit the dynamic behavior of interest in the system under consideration. This is one of the main conclusions of this research, and further work is needed to confirm this finding.

7. Summary, Conclusions, and Future Work

7.1. Research Synopsis

This investigation proposes a novel method for estimating the unknown parameters of nonlinear mechanical systems via numerical experiments, combining dynamical simulations with nonlinear regression. More specifically, this study estimates the unknown parameters of single-degree-of-freedom nonlinear mechanical systems using the explicit fourth-order Runge–Kutta method for time-marching numerical solution and the Levenberg–Marquardt nonlinear regression method. The approach proposed in this paper addresses the parametric identification problem for vibrating systems subjected to restoring, viscous, and friction forces arising from springs, dampers, and dry frictional contact.

Two benchmark problems are designed and analyzed for the purposes of this study. In the first example, a mass-spring-damper system with Coulomb friction is considered. In this system, the nonlinearity arises from friction between the cart and the ground. The second example, on the other hand, involves a simple pendulum-damper system with Coulomb friction. In the dynamic behavior of this second system, the nonlinearity is also caused by the large rotations of the pendulum. These mechanical systems serve as case studies in this paper to demonstrate the effectiveness of the proposed approach. In both mechanical systems, the dimensionless damping factors and dry friction coefficients are the unknown parameters to be identified through numerical experiments and nonlinear regression. The numerical datasets for both the nonlinear mechanical systems under study are generated using the Runge–Kutta method, which serves as an integration method for

numerically computing the dynamic behavior of the nonlinear systems under investigation. Additionally, five input force types are analyzed to estimate the dimensionless damping factors and dry friction coefficients of the nonlinear mechanical systems considered as benchmark problems, namely a zero input, a step input, a harmonic input, a linear input, and a chirp input. The significant variability of the time histories used as external input excitations proved to be a key ingredient in the success of the parametric identification procedure devised in this investigation.

7.2. Final Remarks

In dry friction models based on the Coulomb law, the friction force is mathematically represented as a sign function. This inevitably creates a discontinuity at zero relative velocity, which could lead to numerical issues in dynamic simulations if no smoothing or regularization techniques are employed. For example, because the Coulomb term involving the sign function of velocity is not differentiable, it may limit the accuracy of modeling vibrational behavior near the occurrence of the stick-slip phenomenon. Therefore, this issue should be thoroughly examined and resolved when applying Coulomb-based friction force models in computer simulations. However, since the two benchmark problems analyzed in this paper are simple single-degree-of-freedom nonlinear systems, the numerical experiments performed in this study showed that a straightforward MATLAB implementation of the sign function is sufficient to accurately capture the overall nonlinear vibrational behavior of the systems under consideration, including the discontinuity at zero velocity, despite ignoring more complex dynamic responses such as the stick-slip phenomenon and the Stribeck effect.

The numerical results obtained in this paper are evaluated qualitatively and quantitatively using relative error and root-mean-square error as metrics. In particular, while the relative error metric is used for the dimensionless damping factor and dry friction coefficient, the root-mean-square error is used to compare the obtained time responses. The analysis of the numerical results found in this investigation reveals that the identification of the desired unknown parameters, like the dimensionless damping factor and the dry friction coefficients, can be carried out by using the proposed approach based on the Levenberg–Marquardt nonlinear regression method and the explicit Runge–Kutta method for the time integration of the equations of motion. Thus, it is observed that the parameter identification process is significantly effective when the input function varies greatly over time. More specifically, based on the numerical experiments conducted in this work, it can be concluded that the unknown parameters of interest can be successfully estimated using the harmonic, linear, and chirp input functions with minimal error. In particular, although the harmonic, linear, and chirp forcing functions all lead to effective parameter identification, the harmonic excitation yielded the most efficient parameter estimation process. On the other hand, the absence of any external input and the presence of a step input negatively affect the performance of the identification algorithm devised in this work.

7.3. Future Developments

Future studies will focus on implementing the approach explained in this work for mechanical systems with more than one degree of freedom and more complex nonlinearities. More precisely, this will be done to demonstrate that selecting single-degree-of-freedom vibrating systems for the first testing phase of this investigation does not limit the efficacy of the proposed methodology for subsequent stages. Additionally, the primary goal of future work will be to identify the stiffness, damping, and friction coefficients of robotic manipulators, a critical preliminary step in developing a compelling control logic for friction compensation. Furthermore, in future research focused on the nonlinear dynamics

and control of robotic manipulators, instead of relying on numerical results from computer simulations, as was done in this study, torque and encoder data measured from the joints are planned to be used as input and output, respectively. Another possible direction for future research is a detailed robustness analysis of the proposed identification procedure with respect to measurement noise in experimental measurements and its effects on the estimated damping factor and friction coefficients of nonlinear vibrating mechanical systems.

Although the proposed methodology proved effective through numerical experiments, several research avenues could enhance its scope and robustness. On the modeling side, it is also essential to treat dry friction more comprehensively. In this paper, for simplicity, more complex friction models, including the Stribeck model and some versions of the smooth Coulomb model available in the literature, were avoided to facilitate the nonlinear mathematical modeling of the state-space dynamical models. Coulomb friction provides a solid starting point, but accurately capturing pre-sliding hysteresis and velocity-dependent effects requires models like Stribeck curves, LuGre or Dahl dynamic friction models, or other more complex state-space formulations. Incorporating these models, along with temperature and load-dependent effects, will improve the accuracy of capture for stick-slip transitions and reduce structural model errors.

In addition, the numerical integration stage can be improved in both accuracy and efficiency. Substituting fixed-step explicit Runge–Kutta schemes with adaptive embedded methods will optimize discretization and accelerate the main function calls used in nonlinear regression. Furthermore, for systems with stiff modes or discontinuities, event-detected integrators, variational or symplectic integrators for energy conservation, or nonsmooth time-steppers can help prevent integration artifacts that interfere with identification. Finally, the optimization process could also be diversified to perform further numerical experiments. It is well known that the Levenberg–Marquardt method performs well near the basin of attraction of the numerical solutions but may stall when the cost landscape becomes complex due to functional nonsmoothness and parameter couplings. A practical improvement is to implement a multi-start strategy with informed initialization, followed by search refinement. All these aspects will be explored in future research.

Author Contributions: This paper was principally devised and developed by the first author: Ş.İ.L. and by the second author: Ö.E.G. Great support in the development of the research was provided by the third author: R.L.R. and by the fourth author: C.M.P. The detailed review carried out by the fifth author: D.G. considerably improved the quality of the work. The manuscript was written with substantial contributions from all authors. All authors reviewed the methodology, discussed the results, revised the paper content. All authors have read and agreed to the published version of the manuscript.

Funding: This research received no external funding.

Data Availability Statement: The data presented in this study are available from the corresponding author upon reasonable request.

Conflicts of Interest: The authors declare no conflicts of interest.

References

1. Etim, B.; Al-Ghosoun, A.; Renno, J.; Seaid, M.; Mohamed, M.S. Machine learning-based modeling for structural engineering: A comprehensive survey and applications overview. *Buildings* **2024**, *14*, 3515. [CrossRef]
2. Plevris, V.; Georgioudakis, M.; Kioumarsi, M. Computational Methods in Structural Engineering: Current Advances and Future Perspectives. *Computation* **2025**, *13*, 224. [CrossRef]

3. Godarzi, N.; Hejazi, F. A Review of Health Monitoring and Model Updating of Vibration Dissipation Systems in Structures. *CivilEng* **2025**, *6*, 3. [CrossRef]
4. Chen, C.; Wang, Y.; Chen, S.; Fang, B.; Cao, D. Knowledge and data fusion-driven dynamical modeling approach for structures with hysteresis-affected uncertain boundaries. *Nonlinear Dyn.* **2025**, *113*, 4179–4195. [CrossRef]
5. Najera-Flores, D.A.; Jacobs, J.; Dane Quinn, D.; Garland, A.; Todd, M.D. Uncertainty-Aware, Structure-Preserving Machine Learning Approach for Domain Shift Detection From Nonlinear Dynamic Responses of Structural Systems. *ASCE-ASME J. Risk Uncertain. Eng. Syst. Part B Mech. Eng.* **2025**, *11*, 011104. [CrossRef]
6. Samadian, D.; Muhit, I.B.; Dawood, N. Application of data-driven surrogate models in structural engineering: A literature review. *Arch. Comput. Methods Eng.* **2025**, *32*, 735–784. [CrossRef]
7. Guo, X.; Li, H.N.; Zhang, H. Multi-hazard failure analysis and performance evaluation of transmission towers utilizing data-driven probabilistic models subject to combined wind and earthquake. *Structures* **2025**, *77*, 109196. [CrossRef]
8. Rahmani, H.R. *Seismic Control of Structures Using Tuned Mass Dampers*; Springer: Berlin/Heidelberg, Germany, 2024.
9. McNamara, D.; Pandit, A.; Malekjafarian, A. Optimized design of multiple tuned mass dampers for vibration control of offshore wind turbines. *Ocean Eng.* **2024**, *305*, 117912. [CrossRef]
10. Khalil, Z.; Stafford, P.J.; Elghazouli, A.Y. Risk-Based Structural Seismic Response Assessment of Large-Scale Jacket-Supported Offshore Wind Turbines. *Earthq. Eng. Struct. Dyn.* **2025**, *54*, 2044–2061. [CrossRef]
11. Song, W.; Yang, X.; Deng, W.; Cattani, P.; Villecco, F. Remaining useful life prediction for power storage electronic components based on fractional Weibull process and shock Poisson model. *Fractal Fract.* **2024**, *8*, 485. [CrossRef]
12. Song, W.; Zhong, M.; Yang, M.; Qi, D.; Spadini, S.; Cattani, P.; Villecco, F. Remaining Useful Life Prediction of Roller Bearings Based on Fractional Brownian Motion. *Fractal Fract.* **2024**, *8*, 183. [CrossRef]
13. Daiic, P. Determination of reliability of ceramic cutting tools on the basis of comparative analysis of different functions distribution. *Int. J. Qual. Reliab. Manag.* **2001**, *18*, 431–443. [CrossRef]
14. Tomlinson, G.; Hibbert, J. Identification of the dynamic characteristics of a structure with Coulomb friction. *J. Sound Vib.* **1979**, *64*, 233–242. [CrossRef]
15. Kopei, V.; Onysko, O.; Barz, C.; Dašić, P.; Panchuk, V. Designing a multi-agent plm system for threaded connections using the principle of isomorphism of regularities of complex systems. *Machines* **2023**, *11*, 263. [CrossRef]
16. Alic, D.; Miltenovic, A.; Banic, M.; Zafra, R.V. Numerical Investigation of Large Vehicle Aerodynamics Under the Influence of Crosswind. *Spectr. Mech. Eng. Oper. Res.* **2025**, *2*, 13–23. [CrossRef]
17. Vestroni, F.; Casini, P. Effectiveness and optimization of a hysteretic absorber for response mitigation. *Nonlinear Dyn.* **2025**, *113*, 30279–30297. [CrossRef]
18. Dašić, P.; Natsis, A.; Petropoulos, G. Models of reliability for cutting tools: Examples in manufacturing and agricultural engineering. *Stroj. Vestn.-J. Mech. Eng.* **2008**, *54*, 122–130.
19. Onysko, O.; Kopei, V.; Barz, C.; Kusyi, Y.; Baskutis, S.; Bembenek, M.; Dašić, P.; Panchuk, V. Analytical model of tapered thread made by turning from different machinability workpieces. *Machines* **2024**, *12*, 313. [CrossRef]
20. Xinxiu, F.; Qi, W. Research on modeling and simulation of longitudinal vehicle dynamics based on non-smooth dynamics of multibody systems. *Chin. J. Theor. Appl. Mech.* **2015**, *47*, 301–309.
21. Lv, F.; He, W.; Zhao, L. An improved nonlinear multibody dynamic model for a parafoil-UAV system. *IEEE Access* **2019**, *7*, 139994–140009. [CrossRef]
22. Wu, H.; Wang, Z.; Zhou, Z.; Wang, R. Modeling and simulation for multi-rotor fixed-wing UAV based on multibody dynamics. *Xibei Gongye Daxue Xuebao/J. Northwest. Polytech. Univ.* **2019**, *37*, 928–934. [CrossRef]
23. Najafi, A.; Spencer, B.F., Jr. Validation of model-based real-time hybrid simulation for a lightly-damped and highly-nonlinear structural system. *J. Appl. Comput. Mech.* **2021**, *7*, 1252–1265.
24. Moura, C.H.; Viegas, B.M.; Tavares, M.R.; Macêdo, E.N.; Estumano, D.C.; Quaresma, J.N. Parameter Estimation in Population Balance through Bayesian Technique Markov Chain Monte Carlo. *J. Appl. Comput. Mech.* **2021**, *7*, 890–901.
25. Gai, Z.; Wang, J. Research on Dynamic Seal Friction Torque Compensation for a Low-Slow-Small UAV Tracking System. *IEEE Access* **2023**, *11*, 6404–6412. [CrossRef]
26. Cirelli, M.; Autiero, M.; Belfiore, N.P.; Paoli, G.; Pennestrì, E.; Valentini, P.P. Review and comparison of empirical friction coefficient formulation for multibody dynamics of lubricated slotted joints. *Multibody Syst. Dyn.* **2025**, *63*, 83–104. [CrossRef]
27. Wang, K.; Tian, Q. A nonsmooth method for spatial frictional contact dynamics of flexible multibody systems with large deformation. *Int. J. Numer. Methods Eng.* **2023**, *124*, 752–779. [CrossRef]
28. Liu, S.; Chen, G.S. *Dynamics and Control of Robotic Manipulators with Contact and Friction*; John Wiley & Sons: Hoboken, NJ, USA, 2019.

29. Rebelein, C.; Vlacil, J.; Zaeh, M.F. Modeling of the dynamic behavior of machine tools: Influences of damping, friction, control and motion. *Prod. Eng.* **2017**, *11*, 61–74. [CrossRef]
30. Kermani, M.; Patel, R.; Moallem, M. Friction identification in robotic manipulators: Case studies. In Proceedings of the 2005 IEEE Conference on Control Applications, CCA 2005, Toronto, ON, Canada, 28–31 August 2005; pp. 1170–1175.
31. Kermani, M.R.; Patel, R.V.; Moallem, M. Friction Identification and Compensation in Robotic Manipulators. *IEEE Trans. Instrum. Meas.* **2007**, *56*, 2346–2353. [CrossRef]
32. Ju, J.; Zhao, Y.; Zhang, C.; Liu, Y. Vibration suppression of a flexible-joint robot based on parameter identification and fuzzy PID control. *Algorithms* **2018**, *11*, 189. [CrossRef]
33. Kornmaneesang, W.; Chen, S.L. An Efficient Parameter Identification Framework: A Case Study on Robot Manipulators. *IEEE Trans. Instrum. Meas.* **2025**, *74*, 7501812. [CrossRef]
34. Cammarata, A.; Maddio, P.D.; Sinatra, R.; Tian, Y.; Zhao, Y.; Xi, F. Elastostatic analysis of a module-based shape morphing snake-like robot. *Mech. Mach. Theory* **2024**, *194*, 105580. [CrossRef]
35. Pappalardo, C.M.; Isola, G.; Donadio, A.; La Regina, R.; Berardi, V.P.; Guida, D. Technical Design and Virtual Testing of a Dynamic Vibration Absorber for the Vibration Control of a Flexible Structure. *Dynamics* **2025**, *5*, 19. [CrossRef]
36. Pappalardo, C.M.; La Regina, R.; Guida, D. Multibody modeling and nonlinear control of a pantograph scissor lift mechanism. *J. Appl. Comput. Mech.* **2023**, *9*, 129–167.
37. Palli, G.; Strano, S.; Terzo, M. A novel adaptive-gain technique for high-order sliding-mode observers with application to electro-hydraulic systems. *Mech. Syst. Signal Process.* **2020**, *144*, 106875. [CrossRef]
38. De Simone, M.C.; Veneziano, S.; Pace, R.; Guida, D. Multibody Analysis of Sloshing Effect in a Glass Cylinder Container for Visual Inspection Activities. *Appl. Sci.* **2024**, *14*, 4522. [CrossRef]
39. Razmjooei, H.; Palli, G.; Strano, S.; Tordela, C. Development of sliding mode observers for estimating sideslip angle and lateral forces in road vehicles. *Trans. Inst. Meas. Control* **2025**. [CrossRef]
40. Marotta, R.; Strano, S.; Terzo, M.; Tordela, C. Enhancing Roll Reduction in Road Vehicles on Uneven Surfaces through the Fusion of Proportional Control and Reinforcement Learning. *SAE Int. J. Veh. Dyn. Stab. NVH* **2024**, *9*, 105–120. [CrossRef]
41. Genovese, A.; Strano, S.; Terzo, M. Design and multi-physics optimization of an energy harvesting system integrated in a pneumatic suspension. *Mechatronics* **2020**, *69*, 102395. [CrossRef]
42. Romano, L.; Sakhnevych, A.; Strano, S.; Timpone, F. A hybrid tyre model for in-plane dynamics. *Veh. Syst. Dyn.* **2019**, *58*, 1123–1145. [CrossRef]
43. De Simone, M.C.; Veneziano, S.; Guida, D. Design of a non-back-drivable screw jack mechanism for the hitch lifting arms of electric-powered tractors. *Actuators* **2022**, *11*, 358. [CrossRef]
44. Archontoulis, S.V.; Miguez, F.E. Nonlinear regression models and applications in agricultural research. *Agron. J.* **2015**, *107*, 786–798. [CrossRef]
45. Pappalardo, C.M.; Califano, F.; Lok, S.I.; Guida, D. A systematic computational and experimental study of the principal data-driven identification procedures. Part I: Analytical methods and computational algorithms. *J. Appl. Comput. Mech.* **2023**, *9*, 529–549.
46. Pappalardo, C.M.; Califano, F.; Lok, S.I.; Guida, D. A systematic computational and experimental study of the principal data-driven identification procedures. Part II: Numerical analysis and experimental testing. *J. Appl. Comput. Mech.* **2023**, *9*, 550–589.
47. Calabrese, A.; Quaglini, V.; Strano, S.; Terzo, M. Online estimation of the friction coefficient in sliding isolators. *Struct. Control Health Monit.* **2020**, *27*, e2459. [CrossRef]
48. Calabrese, A.; Losanno, D.; Barjani, A.; Spizzuoco, M.; Strano, S. Effects of the long-term aging of glass-fiber reinforced bearings (FRBs) on the seismic response of a base-isolated residential building. *Eng. Struct.* **2020**, *221*, 110735. [CrossRef]
49. Zardian, M.G.; Darus, I.Z.M.; Miveh, M.R. System identification and intelligent control of flexible manipulator system. *J. Soft Comput. Decis. Support Syst.* **2015**, *3*, 44–52.
50. Kumar, P.R.; Bandyopadhyay, B. The forward kinematic modeling of a Stewart platform using NLARX model with wavelet network. In Proceedings of the 2013 11th IEEE International Conference on Industrial Informatics (INDIN), Bochum, Germany, 29–31 July 2013; pp. 343–348.
51. Bartali, L.; Gabiccini, M.; Grabovic, E.; Domenighini, M.; Guiggiani, M. A reduced-order lie group-based race car model for systematic trajectory optimization on 3D tracks. *Meccanica* **2023**, *58*, 1869–1883. [CrossRef]
52. Sahoo, S.K.; Choudhury, B.B.; Dhal, P.R. Exploring the role of robotics in maritime technology: Innovations, challenges, and future prospects. *Spectr. Mech. Eng. Oper. Res.* **2024**, *1*, 159–176. [CrossRef]
53. Cammarata, A.; Sinatra, R.; Rigato, R.; Maddio, P.D. Tie-system calibration for the experimental setup of large deployable reflectors. *Machines* **2019**, *7*, 23. [CrossRef]

54. Marano, D.; Cammarata, A.; Fichera, G.; Sinatra, R.; Prati, D. Modeling of a three-axes MEMS gyroscope with feedforward PI quadrature compensation. In Proceedings of the Advances on Mechanics, Design Engineering and Manufacturing: Proceedings of the International Joint Conference on Mechanics, Design Engineering & Advanced Manufacturing (JCM 2016), Catania, Italy, 14–16 September 2016; Springer: Cham, Switzerland, 2016; pp. 71–80.
55. Seber, G.A.F.; Wild, C.J. *Nonlinear Regression*; Wiley: Hoboken, NJ, USA, 1989. [CrossRef]
56. Gavin, H.P. The Levenberg-Marquardt algorithm for nonlinear least squares curve-fitting problems. *Dep. Civ. Environ. Eng. Duke Univ. August* **2019**, *3*, 1–23.
57. Lourakis, M.I. A brief description of the Levenberg-Marquardt algorithm implemented by levmar. *Found. Res. Technol.* **2005**, *4*, 1–6.
58. Madsen, K.; Nielsen, H.B.; Tingleff, O. Methods for non-linear least squares problems. In *Informatics and Mathematical Modeling*; Technical University of Denmark: Kongens Lyngby, Denmark, 2004.
59. Nicolini, A.; Mocera, F.; Soma, A. Multibody simulation of a tracked vehicle with deformable ground contact model. *Proc. Inst. Mech. Eng. Part K J. Multi-Body Dyn.* **2019**, *233*, 152–162. [CrossRef]
60. Escalona, J.L.; Recuero, A.M. A bicycle model for education in multibody dynamics and real-time interactive simulation. *Multibody Syst. Dyn.* **2012**, *27*, 383–402. [CrossRef]
61. Press, W.H. *Numerical Recipes 3rd Edition: The Art of Scientific Computing*; Cambridge University Press: Cambridge, UK, 2007.
62. LeVeque, R.J. *Finite Volume Methods for Hyperbolic Problems*; Cambridge University Press: Cambridge, UK, 2002; Volume 31.
63. Süli, E.; Mayers, D.F. *An Introduction to Numerical Analysis*; Cambridge University Press: Cambridge, UK, 2003.
64. Hamming, R. *Numerical Methods for Scientists and Engineers*; Courier Corporation: Chelmsford, MA, USA, 2012.
65. Eichmeir, P.; Jech, M.; Vorlaufer, G.; Nachbagauer, K. The adjoint gradient computation for parameter identification of a tribology test bench. *Forsch. Im Ingenieurwesen* **2025**, *89*, 152. [CrossRef]
66. Pappalardo, C.M.; Guida, D. Use of the adjoint method for controlling the mechanical vibrations of nonlinear systems. *Machines* **2018**, *6*, 19. [CrossRef]
67. Bewley, T.; Luchini, P.; Pralits, J. Methods for solution of large optimal control problems that bypass open-loop model reduction. *Meccanica* **2016**, *51*, 2997–3014. [CrossRef]
68. Eichmeir, P.; Nachbagauer, K.; Steiner, W. The adjoint method for optimal control of multibody systems for free end time and final constraints. *Multibody Syst. Dyn.* **2025**, 1–19. [CrossRef]
69. Huang, X.; Cao, H.; Jia, B. Optimization of Levenberg Marquardt algorithm applied to nonlinear systems. *Processes* **2023**, *11*, 1794. [CrossRef]
70. Yuan, Y.X. Recent advances in numerical methods for nonlinear equations andnonlinear least squares. *Numer. Algebr. Control Optim.* **2011**, *1*, 15–34. [CrossRef]
71. Bellavia, S.; Gratton, S.; Riccietti, E. A Levenberg–Marquardt method for large nonlinear least-squares problems with dynamic accuracy in functions and gradients. *Numer. Math.* **2018**, *140*, 791–825. [CrossRef]
72. Xu, K.; Cao, M.; Xue, S.; Li, D.; Li, X.; Yi, Z. Single accelerometer-based inter-story drift reconstruction of soft-story for shear structures with innovative transformation function. *Mech. Syst. Signal Process.* **2025**, *222*, 111800. [CrossRef]
73. Shabana, A.A. *Dynamics of Multibody Systems*; Cambridge University Press: Cambridge, UK, 2020.
74. Negrean, I.; Crișan, A.; Șerdean, F.; Vlase, S. New formulations on kinetic energy and acceleration energies in applied mechanics of systems. *Symmetry* **2022**, *14*, 896. [CrossRef]
75. Bratu, P. Multibody system with elastic connections for dynamic modeling of compactor vibratory rollers. *Symmetry* **2020**, *12*, 1617. [CrossRef]
76. Marques, F.; Flores, P.; Claro, J.P.; Lankarani, H.M. Modeling and analysis of friction including rolling effects in multibody dynamics: A review. *Multibody Syst. Dyn.* **2019**, *45*, 223–244. [CrossRef]
77. Marques, F.; Flores, P.; Pimenta Claro, J.; Lankarani, H.M. A survey and comparison of several friction force models for dynamic analysis of multibody mechanical systems. *Nonlinear Dyn.* **2016**, *86*, 1407–1443. [CrossRef]
78. Pennestrì, E.; Valentini, P.; Vita, L. Multibody dynamics simulation of planar linkages with Dahl friction. *Multibody Syst. Dyn.* **2007**, *17*, 321–347. [CrossRef]
79. Pennestrì, E.; Rossi, V.; Salvini, P.; Valentini, P.P. Review and comparison of dry friction force models. *Nonlinear Dyn.* **2016**, *83*, 1785–1801. [CrossRef]
80. Piedbœuf, J.C.; De Carufel, J.; Hurteau, R. Friction and stick-slip in robots: Simulation and experimentation. *Multibody Syst. Dyn.* **2000**, *4*, 341–354. [CrossRef]
81. The MathWorks Inc. Translational Friction. 2022. Available online: https://www.mathworks.com/help/simscape.html (accessed on 16 December 2025).
82. The MathWorks Inc. Rotational Friction. 2022. Available online: https://www.mathworks.com/help/simscape.html (accessed on 16 December 2025).

83. Gloth, G.; Sinapius, M. Analysis of swept-sine runs during modal identification. *Mech. Syst. Signal Process.* **2004**, *18*, 1421–1441. [CrossRef]
84. Avitabile, P. *Modal Testing: A Practitioner's Guide*; John Wiley & Sons: Hoboken, NJ, USA, 2017.
85. Nelles, O. Nonlinear system identification. *Meas. Sci. Technol.* **2002**, *13*, 646. [CrossRef]

Disclaimer/Publisher's Note: The statements, opinions and data contained in all publications are solely those of the individual author(s) and contributor(s) and not of MDPI and/or the editor(s). MDPI and/or the editor(s) disclaim responsibility for any injury to people or property resulting from any ideas, methods, instructions or products referred to in the content.